Supporting Information

Z-Form Adoption of Nucleic Acid is a Multi-Step Process Which Proceeds Through a Melted Intermediate

Parker J. Nichols[1], Jeffrey B. Krall[1], Morkos A. Henen[1,2], Robb Welty[1], Andrea MacFadden[1], Quentin Vicens[1,3,4*], and Beat Vögeli[1*]

1. Department of Biochemistry and Molecular Genetics, University of Colorado Denver School of Medicine, Aurora, Colorado, 80045, USA.
2. Faculty of Pharmacy, Mansoura University, Mansoura, 35516, Egypt.
3. RNA Bioscience Initiative, University of Colorado Denver School of Medicine, Aurora, Colorado, 80045, USA.
4 Present address: Department of Biology and Biochemistry, Center for Nuclear Receptors and Cellular Signaling, University of Houston, Houston, Texas 77204, USA.
4. *Correspondence: beat.vogeli@cuanschutz.edu, qvicens@uh.edu; Tel.: +1 (303) 724-1627 (B.V.); +1 (346) 352-9827 (Q.V.)

Materials and Methods

DNA and RNA constructs and preparation

All DNA constructs except for the 8mG4 $d(CpG)_3$ were synthesized by Integrated DNA Technologies. All RNA constructs except for the 8mG4 $r(CpG)_3$ were synthesized by Dharmacon (a part of Horizon Discovery). Both the 8mG4 $d(CpG)_3$ and 8mG4 $r(CpG)_3$ constructs were synthesized by the Yale School of Medicine oligo synthesis resource. All nucleic acid constructs in this study were heat annealed prior to use at 95°C for five minutes, followed by slow cooling at room temperature for 30 min.

For NMR experiments, the constructs were dialyzed into 20 mM potassium phosphate, 25 mM NaCl (pH 6.4), except for the 8mG4 $r(CpG)_3$, ^{15}N, ^{13}C isotopically labeled G4 $r(CpG)_3$, and locked $(CpG)_3$ constructs, which also had 0.5 mM EDTA. The samples were concentrated using Amicon 3 kDa cutoff centrifugal filters (Millipore-Sigma). All NMR DNA/RNA were then lyophilized and resuspended in 300 µL of 99.98% D_2O twice (to remove as much of the water as possible). The samples were then pipetted into 5 mm Shigemi tubes matched to D_2O (Wilmad Glass). The concentrations at which NMR experiments were measured were the following: $r(CpG)_3$, ~3.6 mM; $d(CpG)_3$, ~ 3.9 mM; $d(5mCpG)_3$, ~3.1 mM; $r(CpG)_6$, ~3.7 mM; 8mG4 $d(CpG)_3$, ~2.3 mM; 8mG4 $r(CpG)_3$, ~2.5 mM. The concentration of the isotopically ^{15}N, ^{13}C G4 labeled $r(CpG)_3$ construct was 300 µM for the Off-Resonance $R1_\rho$ concentration dependence comparison (Figure 5), and 50 µM for all the Zα titration NMR measurements.

For Circular Dichroism (CD) measurements, all DNA and RNA constructs were resuspended to a final concentration of 50 µM in 20 mM potassium phosphate, 25 mM NaCl (pH 6.4), and 0.5 mM EDTA.

For the Electrophoretic Mobility Shift Assay (EMSA) experiments, 1 µL of 24 µM $r(CpG)_8$ and LNA $(CpG)_8$ were 5'-end labeled with γ-^{32}P-ATP (PerkinElmer) using T4 polynucleotide kinase (NEB) according to the manufacturer's instructions. Reactions were incubated for 1 hour at 37°C and then purified by denaturing polyacrylamide gel electrophoresis. The labeled RNAs were excised from the gel, crush-soaked in DEPC H_2O overnight at 4°C in a thermomixer to elute the RNA, and then filtered to remove the crushed gel pieces. The RNAs were then ethanol precipitated and resuspended in 100 µL of DEPC H_2O and further diluted to achieve a concentration and radioactivity (measured in counts per minute per µL [CPM/µL]) of ~2.4 nM and 4000 cpm/µL, respectively.

Protein expression and purification

The N-terminal Zα domain of *Homo sapiens* ADAR1 in the pet-28a(+) plasmid (N-terminal 6x His-tag and thrombin cleavage site between His tag and the Zα sequence) was a gift from Drs. Peter Dröge and Alekos Athanasiadis and purified as previously described[1–3] with minor modifications. Briefly, the plasmid was transformed and expressed in BL21(DE3) *E. coli*. The cell cultures were grown in Luria Broth (LB) to an OD_{600} of ~0.4 and induced with IPTG to a final concentration of 1 mM and allowed to express Zα for 4 hours at 37°C, then centrifuged to collect the cell pellets. Cell pellets were resuspended in lysis buffer (50 mM Tris-HCl (pH 8.0), 300 mM NaCl, 10 mM imidazole, 1 mM BME) and sonicated. Lysate was centrifuged and the supernatant was applied to a His-trap column, (50 mM Tris-HCl (pH 8.0), 1 M NaCl, 10 mM imidazole, 1 mM BME), and eluted in 20 mL of elution buffer washed with 40 mL of lysis buffer, 80 mL of wash buffer (50 mM Tris-HCl (pH 8.0), 300 mM NaCl, 500 mM imidazole, 1 mM BME). The eluents were concentrated to ~2 mL and applied to a HiLoad 16/600 Superdex 200 prep grade Gel Filtration Column (GE Healthcare) and the peak corresponding to pure protein (which elutes at ~80 mL in 20 mM potassium phosphate (pH 6.4), 300 mM NaCl) was collected and concentrated using an Amicon 3 kDa cutoff centrifugal filter (Millipore-Sigma, Burlington, MA). Zα was dialyzed and concentrated into 20 mM potassium phosphate (pH 6.4), 25 mM, 0.5 mM EDTA and concentrated to 2 mM using an Amicon 3 kDa cutoff centrifugal filter (Millipore-Sigma), after which D_2O was added to 5%. Subsequent dilutions were made in 20 mM potassium phosphate (pH 6.4), 25 mM, 0.5 mM EDTA as needed for the different experiments. The Zβ and ZαY177A mutant domains were purified in the same manner as Zα.

Circular Dichroism

All CD measurements were collected using a JASCO J-815 CD spectrometer (run using Spectra Manager version 2 (JASCO)) in a 0.1 cm quartz cuvette. For melting temperature measurements, spectra were collected in 1-nm steps from 320 to 220 nm from 5 to 95°C in 5°C increments. Two scans were acquired and averaged. The melting temperature T_M was calculated by fitting the temperature dependent change in the ellipticity to a sigmoidal relationship and reporting the temperature at which the signal was 50% saturated (Figure S2). The values reported are the average of two separate experiments along with the standard deviation. The wavelengths plotted as a function of temperature were 253 nm for DNA and 266 nm for RNA with a few exceptions. For the 8mG4 $d(CpG)_3$ construct, melting was monitored at 295 nm. For the 8mG4 $r(CpG)_3$ construct, melting was monitored at both 266 and 295 nm, which had different midpoint transitions. The locked constructs were monitored at 266 nm since they exclusively adopt the A-form conformation[4]. All T_M values can be found in Table 1.

For Z-form midpoint determination, spectra were collected in 1-nm steps from 320 to 220 nm at increasing concentrations of $NaClO_4$, which is known to efficiently induce the Z-conformation in DNA and RNA[5] (Figure S1A). Two scans were acquired and averaged. The midpoint for Z-form adoption was calculated similarly as for the T_M, by plotting the ellipticity at 266 nm for DNA and 285 nm for RNA (wavelengths which reflect Z-DNA and Z-RNA[3,6–8]) as a function of [$NaClO_4$] and fitting the data to a sigmoidal curve and reporting the [$NaClO_4$] required to reach half saturation into the Z-conformation (Figure S1B). All midpoint values (the average of two separate experiments along with the standard deviation) can be found in Table 1.

Z-form adoption by Zα (not the time-course studies) was carried out by incubating saturating amounts of Zα with the DNA or RNA constructs at a 1:(2n) molar ratio of nucleic acid:Zα, where n is the number of Zα binding sites on the duplex, for 1 hour at 42°C before cooling to the experiment temperature and measuring (Figure S21). (i.e., 4 Zα monomers per 6 base pairs in $(CpG)_n$ sequence contexts[9,10]). Spectra were collected in 1-nm steps from 320 to 220 nm, again with an average of two scans.

CD time-courses were measured by rapidly pipetting saturating amounts of Zα into the 50 μM nucleic acid sample to a final 1:(2n) molar ratio of nucleic acid:Zα and then measuring the ellipticity at 266 nm for DNA or 285 nm for RNA, the hybrid $(dCprG)_6$, or the locked nucleic acid constructs. The deadtime between adding Zα and beginning the CD measurement was ~5 seconds. Time-courses were measured over different lengths of time depending on the temperature. For the DNA constructs (which proceeded relatively quickly), we measured time courses at 5°C for 6 h, 15°C for 2 h, and 25°C for 1 h. For the RNA constructs, we measured time courses at 25°C for 6 h, 42°C for 2 h, and 55°C for 1 h (Figure S22). 42°C was chosen

instead of 45°C as it allows for direct comparisons to previously measured nucleic acid:Zα complexes[6] and matches our NMR measurements. Zα and nucleic acid samples were pre-incubated at the measurement temperatures for 10 minutes before mixing.

Pseudo-first order association constants (k) were acquired by fitting the time-course data to a one phase association equation using Prism. Arrhenius plots were constructed from the observed rate constants' temperature dependence to extract the transitions' activation energy (E_A) (Figure S24).

Electrophoretic Mobility Shift Assays (EMSA)

The γ-^{32}P-ATP labeled r(CpG)$_8$ RNA and (CpG)$_8$ LNA were diluted to a concentration of 240 pM (and 400 CPM/μL) in DEPC H_2O, denatured at 85°C for 10 minutes, and allowed to refold at room temperature for 10 minutes. The Zα, Zβ, and ZαY177A protein stocks at 1.25 mM were serially diluted (5X dilutions) in 20 mM potassium phosphate (pH 7.0), 100 mM NaCl, 1 mM DTT, 0.5 mM EDTA to make final concentrations of: 1.25 mM, 250 μM, 50 μM, 10 μM, 2 μM, 400 nM, and 80 nM. The cold r(CpG)$_8$ was refolded the same way as the labeled RNA and serially diluted from a 100 μM stock to make the following concentrations in DEPC H_2O: 10 μM, 1 μM, 100 nM, 10 nM, 5 nM, 2 nM, 1 nM, 250 pM. The labeled RNA and LNA were then diluted 10X from its 240 pM stock to a final concentration of 24 pM (about 400 CPM per well) along with 1 μL of the protein (10X dilution) or cold RNA stocks (either Zα, Zβ, or ZαY177A or cold r(CpG)$_8$) and 5 μL of a 2X buffer stock (40 mM potassium phosphate (pH 7.0), 200 mM NaCl, 2 mM DTT, 1 mM EDTA) and raised to a total volume of 10 μL using DEPC H_2O. The samples were then incubated at 37°C for 30 minutes, after which 10 μL of 2X native loading buffer (62.5 mM Tris-HCl pH (6.8), 25% glycerol, and 1% bromophenol blue) was added to each sample. For the EMSA time course, 1 μL of 10 μM of Zα (final concentration of 1 μM) was added to γ-^{32}P-ATP labeled r(CpG)$_8$ RNA in 5 minute intervals and then incubated at 37°C until 30 minutes had passed, at which point 1 μL of 50 μM and 250 μM Zα was added to the two of the tubes and then 2X loading buffer was added to all of the reactions. There was a 5 minute deadtime to load the gels before the samples were run. All samples were electrophoresed at 250 V for 20 minutes at 4°C on 0.5X TBE, 0.72% crosslinker 8% polyacrylamide native gels. The gels were exposed overnight on a phosphor screen (Molecular Dynamics) and imaged using a Typhoon laser-scanner platform (Cytivia). Band intensity analysis was carried out using FIJI[11].

NMR spectroscopy

All NMR experiments were carried out on a Bruker 600 MHz spectrometer (run using TopSpin 4.2.0 (Bruker)) equipped with a 5/3 mm triple resonance ^{1}H/^{13}C/^{15}N/^{19}F cryoprobe (CP2.1 TCI or Varian 600 MHz spectrometer (run using OpenVNMRJ) equipped with 5 mm triple resonance ^{1}H/^{13}C/^{15}N cold probes with a Z-axis gradient. All ^{1}H carrier frequencies were centered on water unless specified (such as for the Off-Resonance R1$_\rho$ relaxation dispersion experiments, where the ^{1}H carrier is centered on the peak of interest).

DNA and RNA assignment experiments

All ^{1}H,^{13}C-HSQC spectra were measured on the Bruker 600 spectrometer with 512 x 78 complex points, 128 scans, and a 1.5 second recycle delay. For the ^{13}C-HSQC spectra targeting the aromatic region of DNA/RNA, the spectral widths were 25 x 45 ppm for the ^{1}H and ^{13}C dimensions, the carrier frequency for ^{13}C was centered at 148 ppm, and the assumed J_{CH} coupling for magnetization transfer was set to 180 Hz. The ^{13}C-HSQC spectra targeting the ribose region had spectral widths of 25 x 70 ppm for the ^{1}H and ^{13}C dimensions, the carrier frequency for ^{13}C was centered at 88 ppm, and the assumed J_{CH} coupling for magnetization transfer was set to 145 Hz. The ^{13}C-HSQC spectra targeting the methyl region for the modified DNA/RNA complexes had spectral widths of 25 x 45 ppm for the ^{1}H and ^{13}C dimensions, the carrier frequency for ^{13}C was centered at 33 ppm, and the assumed J_{CH} coupling for magnetization transfer was set to 35 Hz (which improves the resolution at the cost of signal-to-noise and helps filter for the methyl peaks).

All non-high salt ^{1}H,^{1}H NOESY and TOCSY experiments were measured on the Bruker 600 spectrometer with 1024 x 400 complex points, 16 scans, and a 2 second recycle delay. The spectral widths

were 11 x 11 ppm for the direct and indirect ^{1}H dimensions. The mixing times for the NOESY and TOCSY experiments were 320 and 60 ms, respectively.

All chemical shifts can be found in Tables S1-S6 and have been deposited to the Biological Magnetic Resonance Bank (BMRB) under accession numbers 52121 ($d(CpG)_3$), 52122 ($d(5mCpG)_3$), 52123 ($r(CpG)_3$), 52124 ($r(CpG)_6$), 52125 (8mG4 $d(CpG)_3$), and 52126 (8mG4 $r(CpG)_3$).

Spectra Assignment

The $r(CpG)_3$, $d(CpG)_3$, $d(5mCpG)_3$, $r(CpG)_6$, 8mG4 $d(CpG)_3$, 8mG4 $r(CpG)_3$ were assigned following the "Assignment walk" strategy discussed here[12]. Briefly, because all these constructs adopt A-form, B-form, or Z-form conformations in solution, they have a continuous set of NOE cross-peaks which allow connections through the helix to be achieved (shown in Figures S4, S5, S7, S9, S12). For B-form and A-form helices, these cross-peaks connect the aromatic H8 and H6 atoms of purines and pyrimidines to the H1′ atoms of adjacent base pairs. Taking the B-/A-form $(CpG)_3$ constructs as an example; the assignment walk is as follows: [H6(n)-H1′(n)-H8(n+1)-H1′(n+1)-H6(n+2)-H1′(n+2), etc]. From here, the proton assignments can be used to assign the corresponding ^{13}C resonances in the ^{1}H,^{13}C-HSQC spectra. Z-form helix assignment is very similar but employs a different atom connectivity due to the unique geometry of Z-form helices[13]. In this case, the NOE connectivity path is [H6(n)-H5′/H5″(n)-H8(n+1)-H1′(n+1)-H6(n+2)]. For cases where ^{1}H peaks were overlapped, the ^{13}C resonances were usually unique allowing for assignment using the chemical shift statistics for DNA and RNA from the BMRB (https://bmrb.io/). The B-form peaks in the 8mG4 $d(CpG)_3$ construct were not strong enough to employ the assignment walk strategy but were completely overlapped with the peaks of the non-modified $d(CpG)_3$ construct except for atoms within or adjacent to the modified guanine (which were mostly minorly perturbed, allowing for assignment). The assignment walk strategy could be employed for both the A-form and Z-form peaks in the 8mG4 $r(CpG)^3$ construct.

Off-Resonance $R1_\rho$ relaxation dispersion experiments

All Off-Resonance $R1_\rho$ relaxation dispersion experiments were performed on the Bruker 600 spectrometer, at either 25°C, 30°C, or 42°C as specified. All experiments were carried out in 99.98% D_2O, as mentioned above. 1D ^{13}C selective Hartman-Hahn magnetization transfers were applied as described here[14–17]. The spin-lock powers (ω) needed to be carefully controlled, and were calibrated accordingly[14,16]. Off-resonance data were collected at 20 various spin-lock offset frequencies (Ω), at five different spin-lock powers (ω), and with five relaxation delays. The five delays were chosen to achieve ~70% loss in signal intensity at the end of the relaxation period. The experimental setup was the same for all residues, but was different between constructs, temperatures, and with the addition of Zα. Details of these experiments are given in Supplementary Table S7.

$R_{1\rho}$ values for each spin-lock power and offset were extracted by fitting the peak intensities as a function of the relaxation delays to a mono-exponential decay using NMRpipe[18]. Errors in the $R_{1\rho}$ values were estimated using a boot-strapping method described here[16,19]. Numerical integration of the Bloch-McConnell equations was used to fit $R_{1\rho}$ values as a function of the spin-lock power and offset to 2-state exchange models as described here[16] and alignment of the magnetization during the Bloch-McConnell fitting process was carried out as previously described[16]. The fitted exchange parameters for the 2-state fits were p_B, k_{exAB}, R_1, R_2, and Δω. Global fits were performed by sharing p_B and k_{exAB} across multiple nuclei. R_1, R_2, and χ^2 values not reported in Table 2 can be found in Table S8. The uncertainties in the exchange parameters were determined using a Monte-Carlo approach[19]. $R_{1\rho}$ dispersion profiles were generated by plotting $(R_2 + R_{ex}) = (R_{1\rho} - R_1\cos^2\theta)/\sin^2\theta$, where θ is the angle between the effective field of the observed resonance and the z-axis, as a function of $\Omega = \omega_{OBS} - \omega_{RF}$, where ω_{OBS} is the Larmor frequency of the observed resonance and ω_{RF} is the angular frequency of the applied spin-lock. These steps are almost entirely performed automatically using the Bloch-McConnell N-State fitting and simulation[20] (BMBS) software provided by the Al-Hashimi lab (https://sites.duke.edu/alhashimilab/resources/).

Supporting tables

(1) Placido, D.; Brown, B. A.; Lowenhaupt, K.; Rich, A.; Athanasiadis, A. A Left-Handed RNA Double Helix Bound by the Zα Domain of the RNA-Editing Enzyme ADAR1. *Structure* **2007**. https://doi.org/10.1016/j.str.2007.03.001.

(2) Kruse, H.; Mrazikova, K.; D'Ascenzo, L.; Sponer, J.; Auffinger, P. Short but Weak: The Z-DNA Lone-Pair···π Conundrum Challenges Standard Carbon Van Der Waals Radii. *Angew. Chemie - Int. Ed.* **2020**. https://doi.org/10.1002/anie.202004201.

(3) Nichols, P. J.; Bevers, S.; Henen, M.; Kieft, J. S.; Vicens, Q.; Vögeli, B. Recognition of Non-CpG Repeats in Alu and Ribosomal RNAs by the Z-RNA Binding Domain of ADAR1 Induces A-Z Junctions. *Nat. Commun.* **2021**. https://doi.org/10.1038/s41467-021-21039-0.

(4) Egli, M.; Minasov, G.; Teplova, M.; Kumar, R.; Wengel, J. X-Ray Crystal Structure of a Locked Nucleic Acid (LNA) Duplex Composed of a Palindromic 10-Mer DNA Strand Containing One LNA Thymine Monomer. *Chem. Commun.* **2001**, No. 7, 651–652. https://doi.org/10.1039/B009447L.

(5) Klump, H. H.; Jovin, T. M. Formation of a Left-Handed RNA Double Helix: Energetics of the A-Z Transition of Poly[r(G-C)] in Concentrated Sodium Perchlorate Solutions. *Biochemistry* **1987**, *26* (16), 5186–5190.

(6) Brown, B. A.; Lowenhaupt, K.; Wilbert, C. M.; Hanlon, E. B.; Rich, A. The Zα Domain of the Editing Enzyme DsRNA Adenosine Deaminase Binds Left-Handed Z-RNA as Well as Z-DNA. *Proc. Natl. Acad. Sci. U. S. A.* **2000**. https://doi.org/10.1073/pnas.240464097.

(7) Kypr, J.; Kejnovská, I.; Renčiuk, D.; Vorlíčková, M. Circular Dichroism and Conformational Polymorphism of DNA. *Nucleic Acids Research*. 2009. https://doi.org/10.1093/nar/gkp026.

(8) Subramani, V. K.; Kim, K. K. Characterization of Z-DNA Using Circular Dichroism. In *Methods in Molecular Biology*; 2023. https://doi.org/10.1007/978-1-0716-3084-6_2.

(9) Placido, D.; Brown 2nd, B. A.; Lowenhaupt, K.; Rich, A.; Athanasiadis, A. A Left-Handed RNA Double Helix Bound by the Z Alpha Domain of the RNA-Editing Enzyme ADAR1. *Structure* **2007**, *15* (4), 395–404. https://doi.org/10.1016/j.str.2007.03.001.

(10) Schwartz, T.; Rould, M. A.; Lowenhaupt, K.; Herbert, A.; Rich, A. Crystal Structure of the Zalpha Domain of the Human Editing Enzyme ADAR1 Bound to Left-Handed Z-DNA. *Science (80-.).* **1999**, *11* (284(5421)), 1841–1845.

(11) Schindelin, J.; Arganda-Carreras, I.; Frise, E.; Kaynig, V.; Longair, M.; Pietzsch, T.; Preibisch, S.; Rueden, C.; Saalfeld, S.; Schmid, B.; Tinevez, J. Y.; White, D. J.; Hartenstein, V.; Eliceiri, K.; Tomancak, P.; Cardona, A. Fiji: An Open-Source Platform for Biological-Image Analysis. *Nature Methods*. 2012. https://doi.org/10.1038/nmeth.2019.

(12) Fürtig, B.; Richter, C.; Wöhnert, J.; Schwalbe, H. NMR Spectroscopy of RNA. *ChemBioChem*. 2003, pp 936–962. https://doi.org/10.1002/cbic.200300700.

(13) Popenda, M.; Milecki, J.; Adamiak, R. W. High Salt Solution Structure of a Left-Handed RNA Double Helix. *Nucleic Acids Res* **2004**, *32* (13), 4044–4054. https://doi.org/10.1093/nar/gkh736.

(14) Hansen, A. L.; Nikolova, E. N.; Casiano-Negroni, A.; Al-Hashimi, H. M. Extending the Range of Microsecond-to-Millisecond Chemical Exchange Detected in Labeled and Unlabeled Nucleic Acids by Selective Carbon R1ρ NMR Spectroscopy. *J. Am. Chem. Soc.* **2009**, *131* (11), 3818–3819. https://doi.org/10.1021/ja8091399.

(15) Xue, Y.; Kellogg, D.; Kimsey, I. J.; Sathyamoorthy, B.; Stein, Z. W.; McBrairty, M.; Al-Hashimi, H. M. Characterizing RNA Excited States Using NMR Relaxation Dispersion. In *Methods in Enzymology*; 2015. https://doi.org/10.1016/bs.mie.2015.02.002.

(16) Rangadurai, A.; Szymaski, E. S.; Kimsey, I. J.; Shi, H.; Al-Hashimi, H. M. Characterizing Micro-to-Millisecond Chemical Exchange in Nucleic Acids Using off-Resonance R1ρ Relaxation Dispersion. *Progress in Nuclear Magnetic Resonance Spectroscopy*. 2019. https://doi.org/10.1016/j.pnmrs.2019.05.002.

(17) Rangadurai, A.; Szymanski, E. S.; Kimsey, I.; Shi, H.; Al-Hashimi, H. M. Probing Conformational Transitions towards Mutagenic Watson–Crick-like G·T Mismatches Using off-Resonance Sugar Carbon R 1ρ Relaxation Dispersion. *J. Biomol. NMR* **2020**. https://doi.org/10.1007/s10858-020-00337-7.

(18) Delaglio, F.; Grzesiek, S.; Vuister, G. W.; Zhu, G.; Pfeifer, J.; Bax, A. NMRPipe: A Multidimensional Spectral Processing System Based on UNIX Pipes. *J. Biomol. NMR* **1995**, *6* (3), 277–293. https://doi.org/10.1007/BF00197809.
(19) Bothe, J. R.; Stein, Z. W.; Al-Hashimi, H. M. Evaluating the Uncertainty in Exchange Parameters Determined from Off-Resonance R1ρ Relaxation Dispersion for Systems in Fast Exchange. *J. Magn. Reson.* **2014**, *244*, 18–29. https://doi.org/10.1016/j.jmr.2014.04.010.
(20) Kimsey, I. J.; Petzold, K.; Sathyamoorthy, B.; Stein, Z. W.; Al-Hashimi, H. M. Visualizing Transient Watson-Crick-like Mispairs in DNA and RNA Duplexes. *Nature* **2015**. https://doi.org/10.1038/nature14227.

Supporting tables

Table S1. Chemical shift assignments for the d(CpG)$_3$ construct.

Residue	^{1}H atom identity	^{1}H chemical shift (ppm)	^{13}C atom identity	^{13}C chemical shift (ppm)
Cyt 1	H5	5.97	C5	99.61
Cyt 1	H6	7.68	C6	143.26
Cyt 1	H1′	5.81	C1′	87.15
Cyt 1	H2′/H2″	2.02/2.46	C2′	39.80
Cyt 1	H3′	4.74	C3′	77.88
Cyt 1	H4′	4.10	C4′	88.18
Cyt 1	H5′/H5″	3.76/3.76	C5′	63.68
Gua 2	H8	8.01	C8	138.10
Gua 2	H1′	5.95	C1′	84.41
Gua 2	H2′/H2″	2.73/2.78	C2′	39.99
Gua 2	H3′	5.02	C3′	79.80
Gua 2	H4′	4.39	C4′	87.29
Gua 2	H5′/H5″	4.14/4.03	C5′	68.30
Cyt 3	H5	5.47	C5	98.70
Cyt 3	H6	7.40	C6	142.42
Cyt 3	H1′	5.79	C1′	86.47
Cyt 3	H2′/H2″	2.08/2.46	C2′	39.80
Cyt 3	H3′	4.90	C3′	77.36
Cyt 3	H4′	4.23	C4′	85.60
Cyt 3	H5′/H5″	4.23/4.18	C5′	67.52
Gua 4	H8	7.96	C8	138.10
Gua 4	H1′	5.93	C1′	84.46
Gua 4	H2′/H2″	2.68/2.75	C2′	40.04
Gua 4	H3′	5.02	C3′	79.80
Gua 4	H4′	4.40	C4′	87.27
Gua 4	H5′/H5″	4.16/4.07	C5′	68.32
Cyt 5	H5	5.50	C5	98.56
Cyt 5	H6	7.37	C6	142.49
Cyt 5	H1′	5.82	C1′	87.16
Cyt 5	H2′/H2″	1.94/2.38	C2′	39.57
Cyt 5	H3′	4.85	C3′	76.48
Cyt 5	H4′	4.19	C4′	85.39
Cyt 5	H5′/H5″	4.24/4.15	C5′	66.95
Gua 6	H8	7.98	C8	139.20
Gua 6	H1′	6.20	C1′	84.65
Gua 6	H2′/H2″	2.41/2.65	C2′	41.75
Gua 6	H3′	4.71	C3′	73.25
Gua 6	H4′	4.21	C4′	87.83
Gua 6	H5′/H5″	4.12/4.10	C5′	67.43

Table S2. Chemical shift assignments for the d(5mCpG)$_3$ construct.

Residue	^{1}H atom identity	^{1}H chemical shift (ppm)	^{13}C atom identity	^{13}C chemical shift (ppm)
Cyt 1	H7$_3$	1.92	C7	30.15
Cyt 1	H6	7.50	C6	140.27
Cyt 1	H1′	5.80	C1′	87.75
Cyt 1	H2′/H2″	2.05/2.42	C2′	39.77
Cyt 1	H3′		C3′	
Cyt 1	H4′	4.07	C4′	88.19
Cyt 1	H5′/H5″	3.72/3.72	C5′	63.89
Gua 2	H8	8.01	C8	138.29
Gua 2	H1′	6.03	C1′	84.58
Gua 2	H2′/H2″	2.70/2.86	C2′	39.93
Gua 2	H3′	5.01	C3′	79.99
Gua 2	H4′	4.39	C4′	87.43

Gua 2	H5′/H5″	4.11/4.01	C5′	68.45
Cyt 3	$H7_3$	1.63	C7	30.27
Cyt 3	H6	7.20	C6	139.05
Cyt 3	H1′	5.71	C1′	86.29
Cyt 3	H2′/H2″	2.09/2.40	C2′	39.69
Cyt 3	H3′	4.87	C3′	77.16
Cyt 3	H4′	4.20	C4′	85.42
Cyt 3	H5′/H5″	4.19/4.16	C5′	67.54
Gua 4	H8	7.93	C8	138.23
Gua 4	H1′	5.98	C1′	84.70
Gua 4	H2′/H2″	2.61/2.79	C2′	40.32
Gua 4	H3′	5.01	C3′	79.99
Gua 4	H4′	4.39	C4′	87.43
Gua 4	H5′/H5″	4.14/4.07	C5′	68.53
Cyt 5	$H7_3$	1.68	C7	30.27
Cyt 5	H6	7.15	C6	139.20
Cyt 5	H1′	5.79	C1′	86.11
Cyt 5	H2′/H2″	1.90/2.31	C2′	39.57
Cyt 5	H3′	4.82	C3′	76.40
Cyt 5	H4′	4.15	C4′	85.17
Cyt 5	H5′/H5″	4.23/4.13	C5′	66.82
Gua 6	H8	7.93	C8	139.26
Gua 6	H1′	6.17	C1′	84.83
Gua 6	H2′/H2″	2.38/2.62	C2′	41.88
Gua 6	H3′	4.66	C3′	73.34
Gua 6	H4′	4.19	C4′	87.93
Gua 6	H5′/H5″	4.10/4.07	C5′	67.55

Table S3. Chemical shift assignments for the 8mG4 $d(CpG)_3$ construct.

Residue	^{1}H atom identity	^{1}H chemical shift (ppm)	^{13}C atom identity	^{13}C chemical shift (ppm)
Z-form: Cyt 1 B-form: Cyt 1	Z-form: H5 B-form: H5	5.81 5.89	Z-form: C5 B-form: C5	99.14 98.96
Z-form: Cyt 1 B-form: Cyt 1	Z-form: H6 B-form: H6	7.47 7.65	Z-form: C6 B-form: C6	142.48 143.46
Z-form: Cyt 1 B-form: Cyt 1	Z-form: H1′ B-form H1′	5.81 5.82	Z-form: C1′ B-form: C1′	89.59 88.18
Z-form: Cyt 1 B-form: Cyt 1	Z-form: H2′/H2″ B-form: H2′/H2″	1.64/2.42 2.01/	Z-form: C2′ B-form: C2′	43.03 40.08
Z-form: Cyt 1 B-form: Cyt 1	Z-form: H3′ B-form: H3′	4.58	Z-form: C3′ B-form: C3′	80.55
Z-form: Cyt 1 B-form: Cyt 1	Z-form: H4′ B-form: H4′	3.66 4.09	Z-form: C4′ B-form: C4′	87.44 88.37
Z-form: Cyt 1 B-form: Cyt 1	Z-form: H5′/H5″ B-form: H5′/H5″	3.12/2.60 3.73/3.73	Z-form: C5′ B-form: C5′	63.53 63.81
Z-form: Gua 2 B-form: Gua 2	Z-form: H8 B-form: H8	7.75 7.99	Z-form: C8 B-form: C8	141.45 138.23
Z-form: Gua 2 B-form: Gua 2	Z-form: H1′ B-form H1′	6.20 5.94	Z-form: C1′ B-form: C1′	87.48 84.52
Z-form: Gua 2 B-form: Gua 2	Z-form: H2′/H2″ B-form: H2′/H2″	2.71/2.78	Z-form: C2′ B-form: C2′	40.28
Z-form: Gua 2 B-form: Gua 2	Z-form: H3′ B-form: H3′	5.01	Z-form: C3′ B-form: C3′	76.87
Z-form: Gua 2 B-form: Gua 2	Z-form: H4′ B-form: H4′	4.18	Z-form: C4′ B-form: C4′	87.00
Z-form: Gua 2 B-form: Gua 2	Z-form: H5′/H5″ B-form: H5′/H5″	4.18/4.12	Z-form: C5′ B-form: C5′	68.60
Z-form: Cyt 3 B-form: Cyt 3	Z-form: H5 B-form: H5	5.09 5.53	Z-form: C5 B-form: C5	98.25 98.71
Z-form: Cyt 3	Z-form: H6	7.36	Z-form: C6	142.20

B-form: Cyt 3	B-form: H6	7.49	B-form: C6	143.40
Z-form: Cyt 3 B-form: Cyt 3	Z-form: H1′ B-form H1′	5.71 5.90	Z-form: C1′ B-form: C1′	89.35 86.93
Z-form: Cyt 3 B-form: Cyt 3	Z-form: H2′/H2″ B-form: H2′/H2″	1.71/2.62	Z-form: C2′ B-form: C2′	44.19
Z-form: Cyt 3 B-form: Cyt 3	Z-form: H3′ B-form: H3′		Z-form: C3′ B-form: C3′	
Z-form: Cyt 3 B-form: Cyt 3	Z-form: H4′ B-form: H4′	3.82 4.19	Z-form: C4′ B-form: C4′	86.32 85.13
Z-form: Cyt 3 B-form: Cyt 3	Z-form: H5′/H5″ B-form: H5′/H5″	2.58/2.49	Z-form: C5′ B-form: C5′	60.52
Z-form: Gua 4 B-form: Gua 4	Z-form: $H9_3$ B-form: $H9_3$	2.54 2.44	Z-form: C9 B-form: C9	15.49 18.77
Z-form: Gua 4 B-form: Gua 4	Z-form: H1′ B-form H1′	6.26 5.91	Z-form: C1′ B-form: C1′	88.59 84.43
Z-form: Gua 4 B-form: Gua 4	Z-form: H2′/H2″ B-form: H2′/H2″	2.72/2.84	Z-form: C2′ B-form: C2′	40.16
Z-form: Gua 4 B-form: Gua 4	Z-form: H3′ B-form: H3′	4.97	Z-form: C3′ B-form: C3′	77.04
Z-form: Gua 4 B-form: Gua 4	Z-form: H4′ B-form: H4′	4.19 4.12	Z-form: C4′ B-form: C4′	88.81 85.16
Z-form: Gua 4 B-form: Gua 4	Z-form: H5′/H5″ B-form: H5′/H5″	3.82/3.78	Z-form: C5′ B-form: C5′	67.30
Z-form: Cyt 5 B-form Cyt 5	Z-form: H5 B-form: H5	5.24 5.57	Z-form: C5 B-form: C5	98.38 98.62
Z-form: Cyt 5 B-form Cyt 5	Z-form: H6 B-form: H6	7.46 7.45	Z-form: C6 B-form: C5	142.45 143.30
Z-form: Cyt 5 B-form Cyt 5	Z-form: H1′ B-form H1′	5.90 5.95	Z-form: C1′ B-form: C1′	89.32 86.82
Z-form: Cyt 5 B-form Cyt 5	Z-form: H2′/H2″ B-form: H2′/H2″	1.76/2.65	Z-form: C2′ B-form: C2′	44.15
Z-form: Cyt 5 B-form Cyt 5	Z-form: H3′ B-form: H3′		Z-form: C3′ B-form: C3′	
Z-form: Cyt 5 B-form Cyt 5	Z-form: H4′ B-form: H4′	3.93 4.17	Z-form: C4′ B-form: C4′	86.53 85.16
Z-form: Cyt 5 B-form Cyt 5	Z-form: H5′/H5″ B-form: H5′/H5″	2.76/2.64	Z-form: C5′ B-form: C5′	67.29
Z-form: Gua 6 B-form: Gua 6	Z-form: H8 B-form: H8	7.82 7.95	Z-form: C8 B-form: C8	142.51 139.39
Z-form: Gua 6 B-form: Gua 6	Z-form: H1′ B-form H1′	6.26 6.19	Z-form: C1′ B-form: C1′	86.03 84.98
Z-form: Gua 6 B-form: Gua 6	Z-form: H2′/H2″ B-form: H2′/H2″	2.44/3.20 2.43/2.65	Z-form: C2′ B-form: C2′	39.79 41.67
Z-form: Gua 6 B-form: Gua 6	Z-form: H3′ B-form: H3′	4.96	Z-form: C3′ B-form: C3′	77.05
Z-form: Gua 6 B-form: Gua 6	Z-form: H4′ B-form: H4′	4.19 4.18	Z-form: C4′ B-form: C4′	86.94 87.98
Z-form: Gua 6 B-form: Gua 6	Z-form: H5′/H5″ B-form: H5′/H5″	4.18/4.11 4.10/4.07	Z-form: C5′ B-form: C5′	68.80 67.71

Table S4. Chemical shift assignments for the $r(CpG)_3$ construct.

Residue	^{1}H atom identity	^{1}H chemical shift (ppm)	^{13}C atom identity	^{13}C chemical shift (ppm)
Cyt 1	H5	6.04	C5	99.02
Cyt 1	H6	8.08	C6	143.01
Cyt 1	H1′	5.62	C1′	93.76
Cyt 1	H2′	4.36	C2′	75.54
Cyt 1	H3′	4.61	C3′	75.49
Cyt 1	H4′	4.37	C4′	84.34
Cyt 1	H5′/H5″	4.07/3.97	C5′	62.00

Gua 2	H8	7.85	C8	136.89
Gua 2	H1′	5.82	C1′	92.38
Gua 2	H2′	4.63	C2′	75.47
Gua 2	H3′	4.60	C3′	73.64
Gua 2	H4′	4.54	C4′	82.28
Gua 2	H5′/H5″	4.54/4.23	C5′	65.46
Cyt 3	H5	5.35	C5	97.74
Cyt 3	H6	7.71	C6	140.91
Cyt 3	H1′	5.59	C1′	93.69
Cyt 3	H2′		C2′	
Cyt 3	H3′	4.48	C3′	72.14
Cyt 3	H4′	4.48	C4′	81.87
Cyt 3	H5′/H5″	4.58/4.18	C5′	64.89
Gua 4	H8	7.59	C8	136.24
Gua 4	H1′	5.75	C1′	92.90
Gua 4	H2′	4.56	C2′	75.40
Gua 4	H3′	4.56	C3′	73.01
Gua 4	H4′	4.49	C4′	81.97
Gua 4	H5′/H5″	4.51/4.15	C5′	65.58
Cyt 5	H5	5.28	C5	97.55
Cyt 5	H6	7.59	C6	140.56
Cyt 5	H1′	5.54	C1′	93.76
Cyt 5	H2′	4.56	C2′	72.49
Cyt 5	H3′	4.49	C3′	72.15
Cyt 5	H4′	4.42	C4′	81.84
Cyt 5	H5′/H5″	4.55/4.10	C5′	64.53
Gua 6	H8	7.65	C8	137.77
Gua 6	H1′	5.88	C1′	91.21
Gua 6	H2′	4.13	C2′	77.91
Gua 6	H3′	4.32	C3′	70.50
Gua 6	H4′	4.25	C4′	83.95
Gua 6	H5′/H5″	4.47/4.08	C5′	65.69

Table S5. Chemical shift assignments for the r(CpG)$_6$ construct.

Residue	^{1}H atom identity	^{1}H chemical shift (ppm)	^{13}C atom identity	^{13}C chemical shift (ppm)
Cyt 1	H5	6.00	C5	99.03
Cyt 1	H6	8.02	C6	143.00
Cyt 1	H1′	5.65	C1′	93.84
Gua 2	H8	7.83	C8	136.74
Gua 2	H1′	5.79	C1′	92.52
Cyt 3,5,7,9	H5	5.23	C5	97.47
Cyt 3,5,7,9	H6	7.64	C6	140.71
Cyt 3,5,7,9	H1′	5.52	C1′	93.82
Gua 4,6,8,10	H8	7.53	C8	136.10
Gua 4,6,8,10	H1′	5.72	C1′	93.09
Cyt 11	H5	5.31	C5	97.68
Cyt 11	H6	7.56	C6	140.50
Cyt 11	H1′	5.60	C8	93.77
Gua 12	H8	7.65	C8	137.61
Gua 12	H1′	5.85	C1′	91.29

Table S6. Chemical shift assignments for the 8mG4 r(CpG)$_3$ construct.

Residue	^{1}H atom identity	^{1}H chemical shift (ppm)	^{13}C atom identity	^{13}C chemical shift (ppm)
Z-form: Cyt 1 A-form: Cyt 1	Z-form: H5 A-form: H5	5.84 6.03	Z-form: C5 A-form: C5	99.72 99.12
Z-form: Cyt 1 A-form: Cyt 1	Z-form: H6 A-form: H6	7.44 8.08	Z-form: C6 A-form: C6	142.40 142.74

Z-form: Cyt 1 A-form: Cyt 1	Z-form: H1′ A-form H1′	5.87 5.60	Z-form: C1′ A-form: C1′	88.82 93.93
Z-form: Cyt 1 A-form: Cyt 1	Z-form: H2′ A-form: H2′	3.83 4.35	Z-form: C2′ A-form: C2′	78.40 75.67
Z-form: Cyt 1 A-form: Cyt 1	Z-form: H3′ A-form: H3′	4.38 4.59	Z-form: C3′ A-form: C3′	79.25 76.54
Z-form: Cyt 1 A-form: Cyt 1	Z-form: H4′ A-form: H4′	3.77 4.37	Z-form: C4′ A-form: C4′	79.65 84.43
Z-form: Cyt 1 A-form: Cyt 1	Z-form: H5′/H5″ A-form: H5′/H5″	3.17/2.38 4.06/3.96	Z-form: C5′ A-form: C5′	63.02 62.07
Z-form: Gua 2 A-form: Gua 2	Z-form: H8 A-form: H8	7.84 7.75	Z-form: C8 A-form: C8	141.42 136.18
Z-form: Gua 2 A-form: Gua 2	Z-form: H1′ A-form H1′	5.83 5.90	Z-form: C1′ A-form: C1′	92.89 93.86
Z-form: Gua 2 A-form: Gua 2	Z-form: H2′ A-form: H2′	4.59 4.73	Z-form: C2′ A-form: C2′	77.07 75.31
Z-form: Gua 2 A-form: Gua 2	Z-form: H3′ A-form: H3′	5.24 4.66	Z-form: C3′ A-form: C3′	76.02 73.85
Z-form: Gua 2 A-form: Gua 2	Z-form: H4′ A-form: H4′	4.32 4.53	Z-form: C4′ A-form: C4′	83.94 82.22
Z-form: Gua 2 A-form: Gua 2	Z-form: H5′/H5″ A-form: H5′/H5″	4.29/4.21 4.52/4.19	Z-form: C5′ A-form: C5′	68.67 65.62
Z-form: Cyt 3 A-form: Cyt 3	Z-form: H5 A-form: H5	5.23 5.14	Z-form: C5 A-form: C5	98.61 97.71
Z-form: Cyt 3 A-form: Cyt 3	Z-form: H6 A-form: H6	7.36 7.67	Z-form: C6 A-form: C6	142.22 142.12
Z-form: Cyt 3 A-form: Cyt 3	Z-form: H1′ A-form H1′	5.90 5.58	Z-form: C1′ A-form: C1′	89.09 94.66
Z-form: Cyt 3 A-form: Cyt 3	Z-form: H2′ A-form: H2′	4.04 4.60	Z-form: C2′ A-form: C2′	78.47 73.72
Z-form: Cyt 3 A-form: Cyt 3	Z-form: H3′ A-form: H3′	4.58 4.35	Z-form: C3′ A-form: C3′	77.24 72.28
Z-form: Cyt 3 A-form: Cyt 3	Z-form: H4′ A-form: H4′	4.04 4.48	Z-form: C4′ A-form: C4′	85.19 82.66
Z-form: Cyt 3 A-form: Cyt 3	Z-form: H5′/H5″ A-form: H5′/H5″	2.65/2.53 4.35/3.85	Z-form: C5′ A-form: C5′	60.54 67.50
Z-form: Gua 4 A-form: Gua 4	Z-form: $H9_3$ A-form: $H9_3$	2.19 2.57	Z-form: C9 A-form: C9	18.30 15.50
Z-form: Gua 4 A-form: Gua 4	Z-form: H1′ A-form H1′	5.87 5.71	Z-form: C1′ A-form: C1′	92.94 89.64
Z-form: Gua 4 A-form: Gua 4	Z-form: H2′ A-form: H2′	4.40 4.65	Z-form: C2′ A-form: C2′	75.47 75.51
Z-form: Gua 4 A-form: Gua 4	Z-form: H3′ A-form: H3′	5.11 4.60	Z-form: C3′ A-form: C3′	75.77 72.74
Z-form: Gua 4 A-form: Gua 4	Z-form: H4′ A-form: H4′	4.30 4.45	Z-form: C4′ A-form: C4′	84.09 83.75
Z-form: Gua 4 A-form: Gua 4	Z-form: H5′/H5″ A-form: H5′/H5″	4.27/4.21 4.27/4.15	Z-form: C5′ A-form: C5′	68.38 67.29
Z-form: Cyt 5 A-form Cyt 5	Z-form: H5 A-form: H5	5.06 5.42	Z-form: C5 A-form: C5	98.75 97.69
Z-form: Cyt 5 A-form Cyt 5	Z-form: H6 A-form: H6	7.23 7.46	Z-form: C6 A-form: C5	142.01 140.04
Z-form: Cyt 5 A-form Cyt 5	Z-form: H1′ A-form H1′	5.79 5.52	Z-form: C1′ A-form: C1′	88.74 94.58
Z-form: Cyt 5 A-form Cyt 5	Z-form: H2′ A-form: H2′	3.97 4.58	Z-form: C2′ A-form: C2′	78.58 73.69
Z-form: Cyt 5 A-form Cyt 5	Z-form: H3′ A-form: H3′	4.53 4.34	Z-form: C3′ A-form: C3′	77.46 73.18
Z-form: Cyt 5 A-form Cyt 5	Z-form: H4′ A-form: H4′	4.01 4.37	Z-form: C4′ A-form: C4′	84.76 82.01
Z-form: Cyt 5	Z-form: H5′/H5″	2.65/2.53	Z-form: C5′	67.54

A-form Cyt 5	A-form: H5′/H5″	4.56/4.09	A-form: C5′	64.42
Z-form: Gua 6 A-form: Gua 6	Z-form: H8 A-form: H8	7.86 7.59	Z-form: C8 A-form: C8	142.86 137.25
Z-form: Gua 6 A-form: Gua 6	Z-form: H1′ A-form H1′	5.85 5.88	Z-form: C1′ A-form: C1′	93.03 91.20
Z-form: Gua 6 A-form: Gua 6	Z-form: H2′ A-form: H2′	5.18 4.14	Z-form: C2′ A-form: C2′	74.55 77.94
Z-form: Gua 6 A-form: Gua 6	Z-form: H3′ A-form: H3′	4.68 4.32	Z-form: C3′ A-form: C3′	72.99 70.66
Z-form: Gua 6 A-form: Gua 6	Z-form: H4′ A-form: H4′	4.29 4.25	Z-form: C4′ A-form: C4′	86.35 84.15
Z-form: Gua 6 A-form: Gua 6	Z-form: H5′/H5″ A-form: H5′/H5″	4.28/4.16 4.45/4.07	Z-form: C5′ A-form: C5′	69.16 65.81

Table S7. Off-Resonance R1$_\rho$ relaxation dispersion experiment spin locks and offsets.

Construct	Temperature (°C)	Spin-lock power (ω, Hz)	Offsets (Ω, Hz)	T_{relax} (ms)
d(CpG)$_3$	25	150	± {10, 50, 100, 150, 200, 250, 300, 350, 400, 450}	0, 16, 32, 64, 96
	25	250	± {10, 83, 166, 249, 332, 415, 498, 581, 664, 747}	0, 16, 32, 64, 96
	25	500	± {10, 167, 334, 501, 668, 835, 1002, 1169, 1336, 1503}	0, 16, 32, 64, 96
	25	1000	± {10, 333, 666, 999, 1332, 1665, 1998, 2331, 2664, 2997}	0, 16, 32, 64, 96
	25	2000	± {10, 667, 1334, 2001, 2668, 3335, 4002, 4669, 5336, 6003}	0, 16, 32, 64, 96
	42	150	± {10, 50, 100, 150, 200, 250, 300, 350, 400, 450}	0, 8, 16, 32, 48
	42	250	± {10, 83, 166, 249, 332, 415, 498, 581, 664, 747}	0, 8, 16, 32, 48
	42	500	± {10, 167, 334, 501, 668, 835, 1002, 1169, 1336, 1503}	0, 8, 16, 32, 48
	42	1000	± {10, 333, 666, 999, 1332, 1665, 1998, 2331, 2664, 2997}	0, 8, 16, 32, 48
	42	2000	± {10, 667, 1334, 2001, 2668, 3335, 4002, 4669, 5336, 6003}	0, 8, 16, 32, 48
d(5mCpG)$_3$	25	150	± {10, 50, 100, 150, 200, 250, 300, 350, 400, 450}	0, 8, 16, 32, 64
	25	250	± {10, 83, 166, 249, 332, 415, 498, 581, 664, 747}	0, 8, 16, 32, 64
	25	500	± {10, 167, 334, 501, 668, 835, 1002, 1169, 1336, 1503}	0, 8, 16, 32, 64
	25	1000	± {10, 333, 666, 999, 1332, 1665, 1998, 2331, 2664, 2997}	0, 8, 16, 32, 64

	25	2000	± {10, 667, 1334, 2001, 2668, 3335, 4002, 4669, 5336, 6003}	0, 8, 16, 32, 64
	42	150	± {10, 50, 100, 150, 200, 250, 300, 350, 400, 450}	0, 8, 16, 32, 64
	42	250	± {10, 83, 166, 249, 332, 415, 498, 581, 664, 747}	0, 8, 16, 32, 64
	42	500	± {10, 167, 334, 501, 668, 835, 1002, 1169, 1336, 1503}	0, 8, 16, 32, 64
	42	1000	± {10, 333, 666, 999, 1332, 1665, 1998, 2331, 2664, 2997}	0, 8, 16, 32, 64
	42	2000	± {10, 667, 1334, 2001, 2668, 3335, 4002, 4669, 5336, 6003}	0, 8, 16, 32, 64
r(CpG)$_3$	25	150	± {10, 50, 100, 150, 200, 250, 300, 350, 400, 450}	0, 16, 32, 64, 80
	25	250	± {10, 83, 166, 249, 332, 415, 498, 581, 664, 747}	0, 16, 32, 64, 80
	25	500	± {10, 167, 334, 501, 668, 835, 1002, 1169, 1336, 1503}	0, 16, 32, 64, 80
	25	1000	± {10, 333, 666, 999, 1332, 1665, 1998, 2331, 2664, 2997}	0, 16, 32, 64, 80
	25	2000	± {10, 667, 1334, 2001, 2668, 3335, 4002, 4669, 5336, 6003}	0, 16, 32, 64, 80
	42	150	± {10, 50, 100, 150, 200, 250, 300, 350, 400, 450}	0, 16, 32, 64, 80
	42	250	± {10, 83, 166, 249, 332, 415, 498, 581, 664, 747}	0, 16, 32, 64, 80
	42	500	± {10, 167, 334, 501, 668, 835, 1002, 1169, 1336, 1503}	0, 16, 32, 64, 80
	42	1000	± {10, 333, 666, 999, 1332, 1665, 1998, 2331, 2664, 2997}	0, 16, 32, 64, 80
	42	2000	± {10, 667, 1334, 2001, 2668, 3335, 4002, 4669, 5336, 6003}	0, 16, 32, 64, 80
r(CpG)$_6$	42	150	± {10, 50, 100, 150, 200, 250, 300, 350, 400, 450}	0, 16, 32, 48, 64
	42	250	± {10, 83, 166, 249, 332, 415, 498, 581, 664, 747}	0, 16, 32, 48, 64
	42	500	± {10, 167, 334, 501, 668, 835, 1002, 1169, 1336, 1503}	0, 16, 32, 48, 64
	42	1000	± {10, 333, 666, 999, 1332, 1665, 1998, 2331, 2664, 2997}	0, 16, 32, 48, 64

	42	2000	± {10, 667, 1334, 2001, 2668, 3335, 4002, 4669, 5336, 6003}	0, 16, 32, 48, 64
8mG4 $d(CpG)_3$	25	150	± {10, 50, 100, 150, 200, 250, 300, 350, 400, 450}	0, 8, 16, 32, 64
	25	250	± {10, 83, 166, 249, 332, 415, 498, 581, 664, 747}	0, 8, 16, 32, 64
	25	500	± {10, 167, 334, 501, 668, 835, 1002, 1169, 1336, 1503}	0, 8, 16, 32, 64
	25	1000	± {10, 333, 666, 999, 1332, 1665, 1998, 2331, 2664, 2997}	0, 8, 16, 32, 64
	25	2000	± {10, 667, 1334, 2001, 2668, 3335, 4002, 4669, 5336, 6003}	0, 8, 16, 32, 64
	30	150	± {10, 50, 100, 150, 200, 250, 300, 350, 400, 450}	0, 8, 16, 32, 64
	30	250	± {10, 83, 166, 249, 332, 415, 498, 581, 664, 747}	0, 8, 16, 32, 64
	30	500	± {10, 167, 334, 501, 668, 835, 1002, 1169, 1336, 1503}	0, 8, 16, 32, 64
	30	1000	± {10, 333, 666, 999, 1332, 1665, 1998, 2331, 2664, 2997}	0, 8, 16, 32, 64
	30	2000	± {10, 667, 1334, 2001, 2668, 3335, 4002, 4669, 5336, 6003}	0, 8, 16, 32, 64
^{15}N, ^{13}C G4 $r(CpG)_3$	25	150	± {10, 50, 100, 150, 200, 250, 300, 350, 400, 450}	0, 8 16, 32, 64
	25	250	± {10, 83, 166, 249, 332, 415, 498, 581, 664, 747}	0, 8 16, 32, 64
	25	500	± {10, 167, 334, 501, 668, 835, 1002, 1169, 1336, 1503}	0, 8 16, 32, 64
	25	1000	± {10, 333, 666, 999, 1332, 1665, 1998, 2331, 2664, 2997}	0, 8 16, 32, 64
	25	2000	± {10, 667, 1334, 2001, 2668, 3335, 4002, 4669, 5336, 6003}	0, 8 16, 32, 64
	42	150	± {10, 50, 100, 150, 200, 250, 300, 350, 400, 450}	0, 8 16, 32, 48
	42	250	± {10, 83, 166, 249, 332, 415, 498, 581, 664, 747}	0, 8 16, 32, 48
	42	500	± {10, 167, 334, 501, 668, 835, 1002, 1169, 1336, 1503}	0, 8 16, 32, 48
	42	1000	± {10, 333, 666, 999, 1332, 1665, 1998, 2331, 2664, 2997}	0, 8 16, 32, 48

	42	2000	± {10, 667, 1334, 2001, 2668, 3335, 4002, 4669, 5336, 6003}	0, 8 16, 32, 48
^{15}N, ^{13}C G4 r(CpG)$_3$ 8:1, 4:1, and 2:1 RNA:Zα	25	150	± {10, 50, 100, 150, 200, 250, 300, 350, 400, 450}	0, 8 16, 24, 32
	25	250	± {10, 83, 166, 249, 332, 415, 498, 581, 664, 747}	0, 8 16, 24, 32
	25	500	± {10, 167, 334, 501, 668, 835, 1002, 1169, 1336, 1503}	0, 8 16, 24, 32
	25	1000	± {10, 333, 666, 999, 1332, 1665, 1998, 2331, 2664, 2997}	0, 8 16, 24, 32
	25	2000	± {10, 667, 1334, 2001, 2668, 3335, 4002, 4669, 5336, 6003}	0, 8 16, 24, 32
^{15}N, ^{13}C G4 r(CpG)$_3$ 1:4 RNA:Zα	25	150	± {10, 50, 100, 150, 200, 250, 300, 350, 400, 450}	0, 8 16, 32, 64
	25	250	± {10, 83, 166, 249, 332, 415, 498, 581, 664, 747}	0, 8 16, 32, 64
	25	500	± {10, 167, 334, 501, 668, 835, 1002, 1169, 1336, 1503}	0, 8 16, 32, 64
	25	1000	± {10, 333, 666, 999, 1332, 1665, 1998, 2331, 2664, 2997}	0, 8 16, 32, 64
	25	2000	± {10, 667, 1334, 2001, 2668, 3335, 4002, 4669, 5336, 6003}	0, 8 16, 32, 64

Table S8. R_1, R_2 and χ^2 values from Off-Resonance $R1_\rho$ relaxation dispersion experiments.

Construct	Residue/Atom identity	Temperature (°C)	R_1 (s^{-1})	R_2 (s^{-1})	χ^2
d(CpG)$_3$	Gua2/C8	42	5.1 ± 0.2	12.5 ± 0.4	1.04
	Cyt3/C6	42	4.2 ± 0.2	10.3 ± 0.6	1.04
	Gua4/C8	42	4.6 ± 0.1	13.0 ± 0.5	1.04
	Cyt5/C6	42	5.2 ± 0.2	12.3 ± 0.3	1.04
d(5mCpG)$_3$	Cyt3/C6	42	4.0 ± 0.5	13.3 ± 1.3	0.81
	Gua4/C8	42	4.5 ± 0.3	10.6 ± 0.6	0.81
	Cyt5/C6	42	5.4 ± 0.3	13.9 ± 1.0	0.81
r(CpG)$_3$	Gua2/C8	42	4.6 ± 0.1	14.5 ± 0.4	1.59
	Cyt3/C6	42	5.3 ± 0.2	13.9 ± 0.3	1.59
	Gua4/C8	42	4.4 ± 0.1	14.1 ± 0.4	1.59
	Cyt5/C6	42	5.0 ± 0.2	15.1 ± 0.3	1.59
	Gua6/C8	42	4.3 ± 0.2	17.1 ± 0.5	1.59

Supporting figures

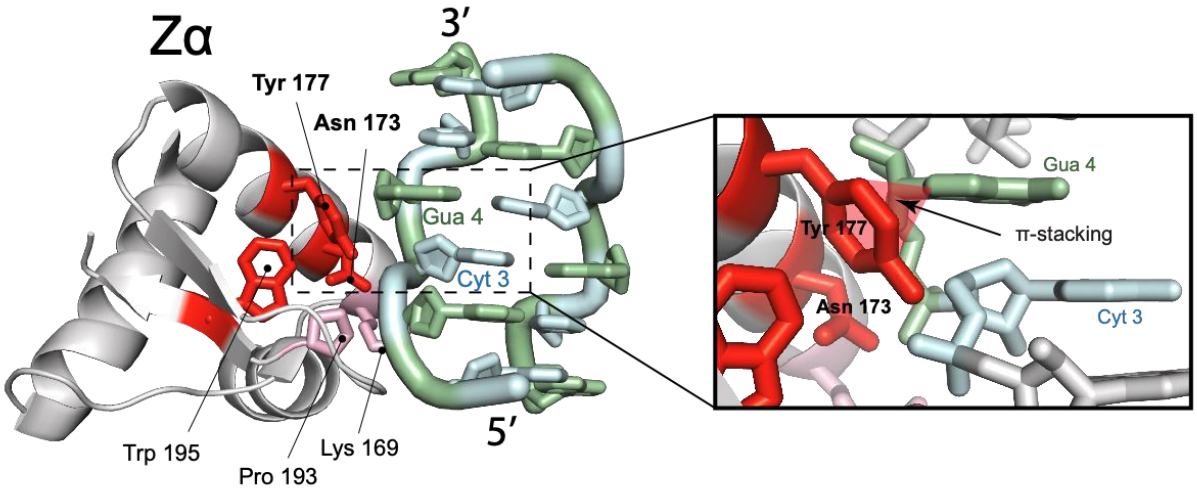

Figure S1. Features of Z-form adoption in the presence of Zα. Zα stabilizes Z-DNA and Z-RNA by making specific contacts with the unique features of the Z-form helix. Highlighted are some of the most critical Zα residues interacting with r(CpG)$_3$ duplex (PDB ID: 2GXB[1]), including Tyrosine 177 which makes a CH–π interaction with the guanine in the *syn* conformation, thereby stabilizing it[1].

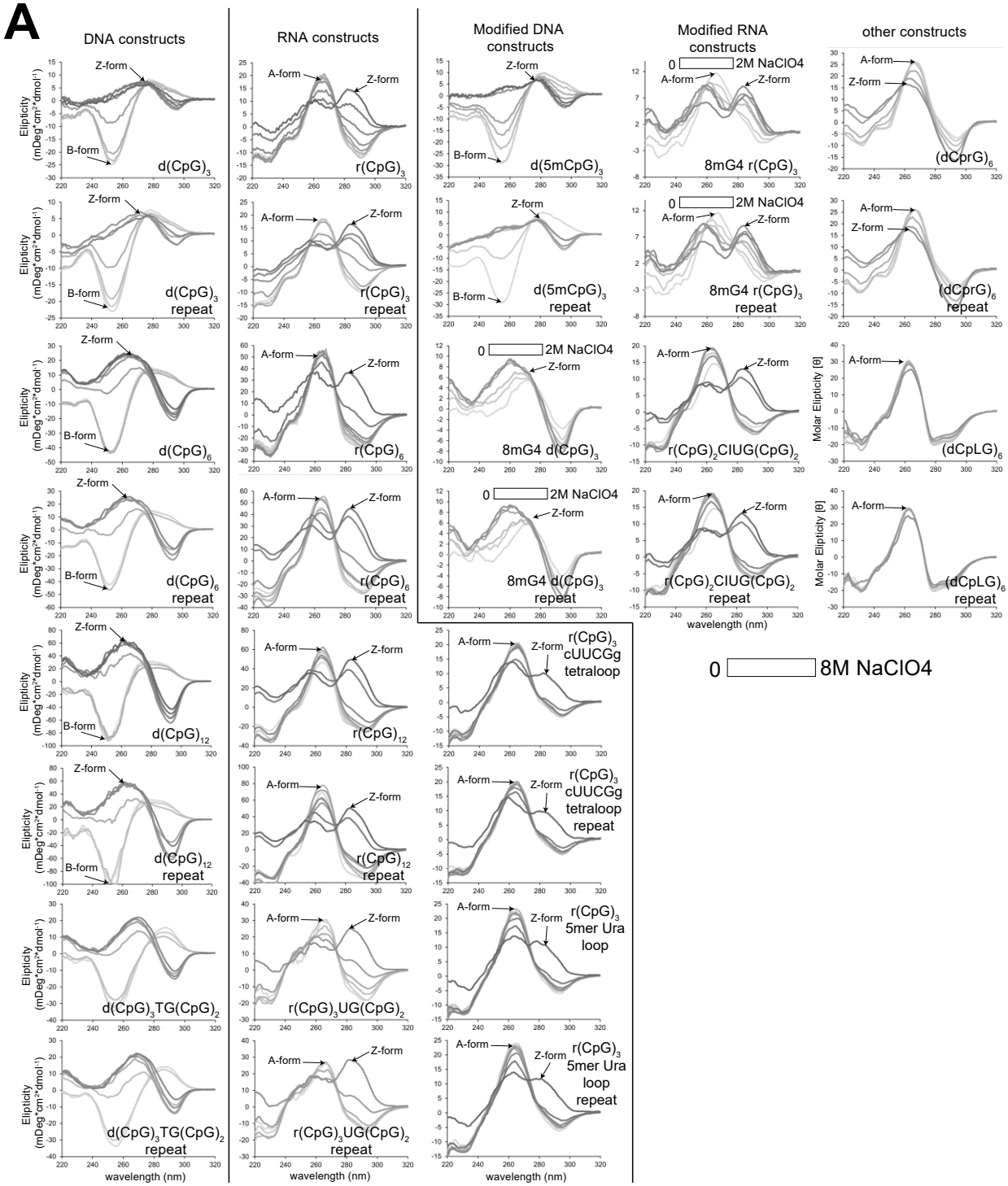
A
DNA constructs
RNA constructs
Modified DNA constructs
Modified RNA constructs
other constructs
Ellipticity (mDeg*cm2*dmol-1)
Molar Ellipticity [θ]
wavelength (nm)
Z-form
B-form
A-form
d(CpG)3
r(CpG)3
d(5mCpG)3
8mG4 r(CpG)3
(dCprG)6
d(CpG)3 repeat
r(CpG)3 repeat
d(5mCpG)3 repeat
8mG4 r(CpG)3 repeat
(dCprG)6 repeat
d(CpG)6
r(CpG)6
8mG4 d(CpG)3
r(CpG)2ClUG(CpG)2
(dCpLG)6
d(CpG)6 repeat
r(CpG)6 repeat
8mG4 d(CpG)3 repeat
r(CpG)2ClUG(CpG)2 repeat
(dCpLG)6 repeat
d(CpG)12
r(CpG)12
r(CpG)3 cUUCGg tetraloop
d(CpG)12 repeat
r(CpG)12 repeat
r(CpG)3 cUUCGg tetraloop repeat
d(CpG)3TG(CpG)2
r(CpG)3UG(CpG)2
r(CpG)3 5mer Ura loop
d(CpG)3TG(CpG)2 repeat
r(CpG)3UG(CpG)2 repeat
r(CpG)3 5mer Ura loop repeat
0
2M NaClO4
8M NaClO4

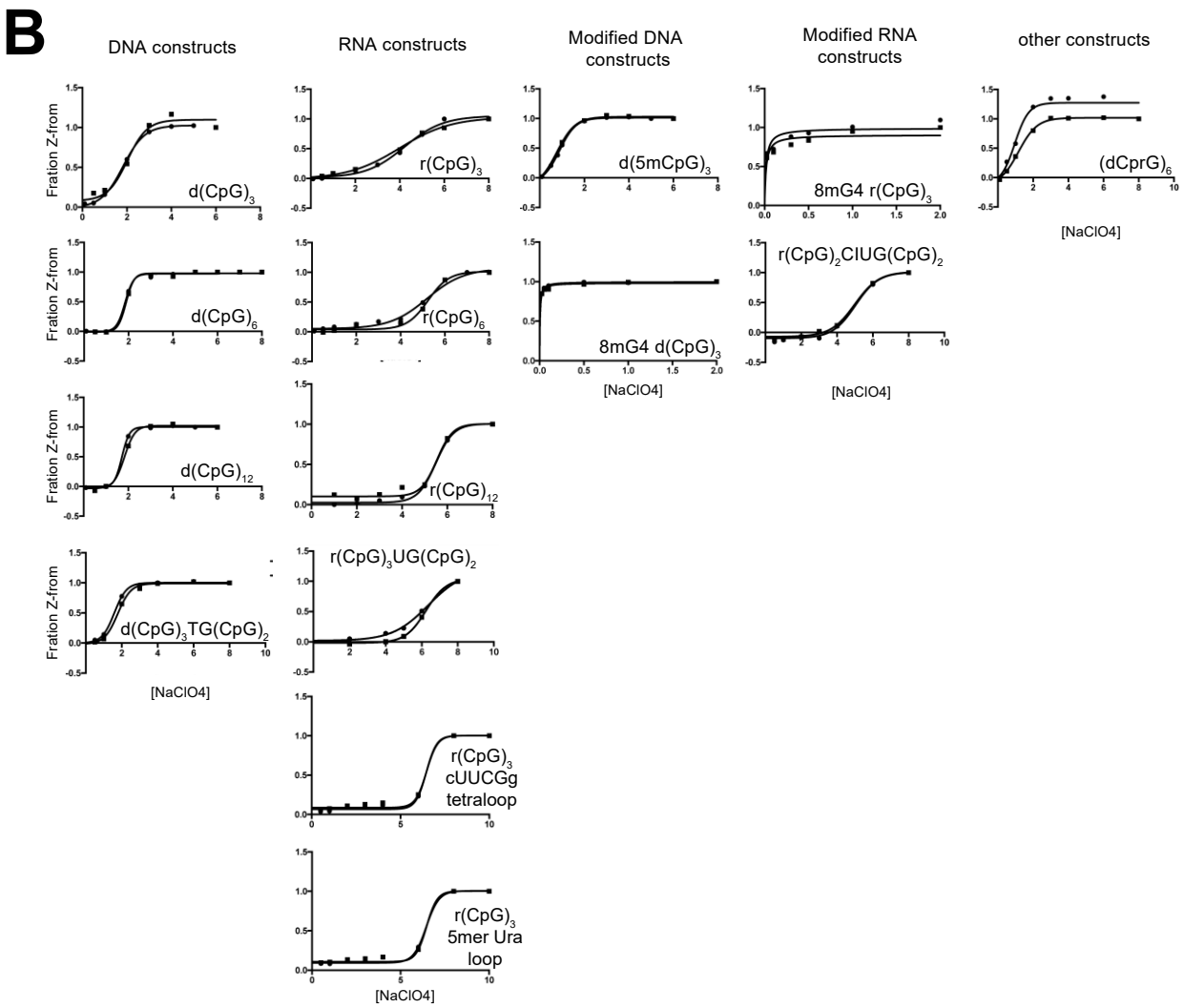

Figure S2. $NaClO_4$ titrations and Z-form midpoints for all the tested d(CpG) and r(CpG) constructs. (a) Circular dichroism spectra covering wavelengths of 320-220 nm from titrations of $NaClO_4$ into the different d(CpG) and r(CpG) constructs used in this study. Spectra are colored as a gradient with low salt spectra being lighter and increasing salt concentrations becoming darker. Each measurement was repeated once. (b) The fraction of Z-form was calculated by following change in the ellipticity at 266 nm for DNA and 285 nm for RNA, and $NaClO_4$ Z-form midpoints were fit as described in the Materials and Methods. Fitted values can be found in Table 1.

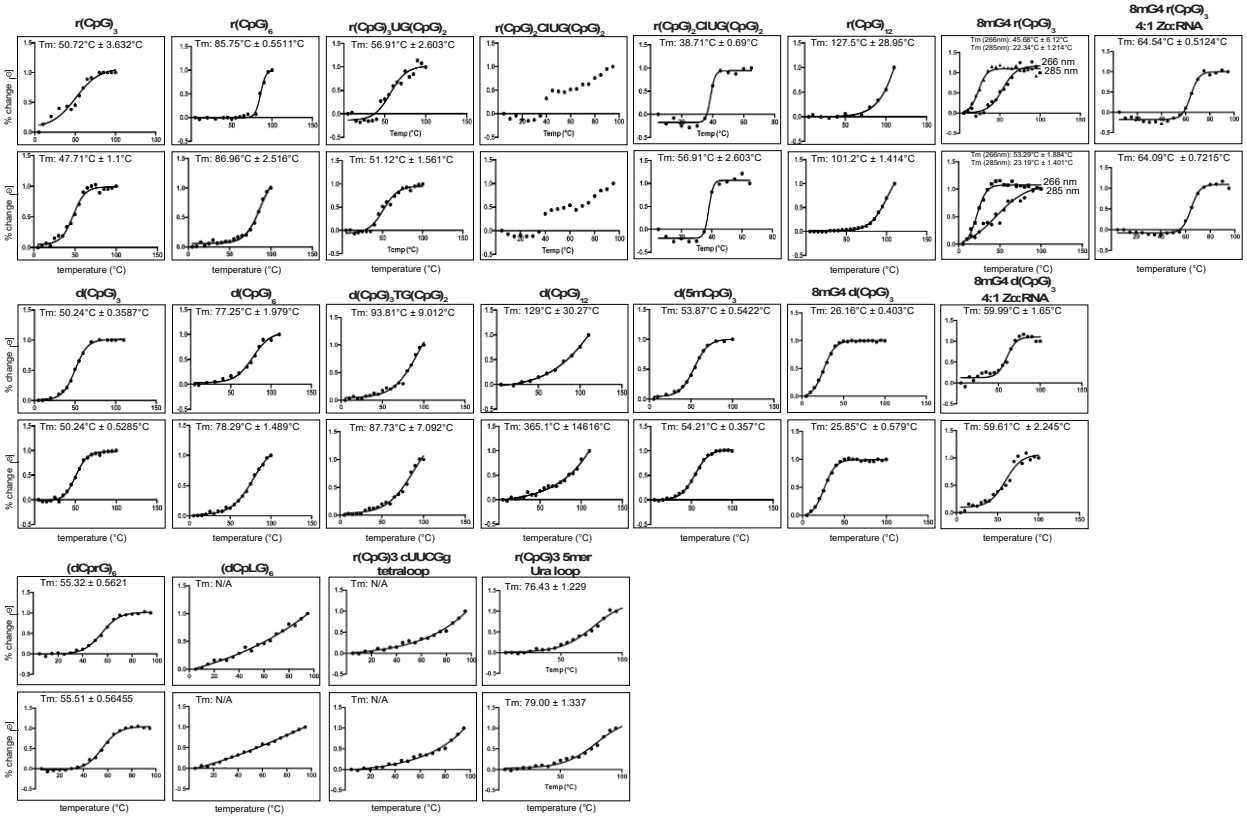

Figure S3. Melting temperatures of all DNA and RNA constructs from this study. The melting temperatures of all DNA and RNA constructs used in this study were measured by following the temperature dependent change in the ellipticity at 253 nm for DNA and 266 nm for RNA with a few exceptions. For the 8mG4 $d(CpG)_3$ construct, melting was monitored at 295 nm. For the 8mG4 $r(CpG)_3$ construct, melting was monitored at both 266 and 295 nm, which had different midpoint transitions. The locked constructs were monitored at 266 nm, since they exclusively adopt the A-form conformation[2]. T_M values are reported in Table 1.

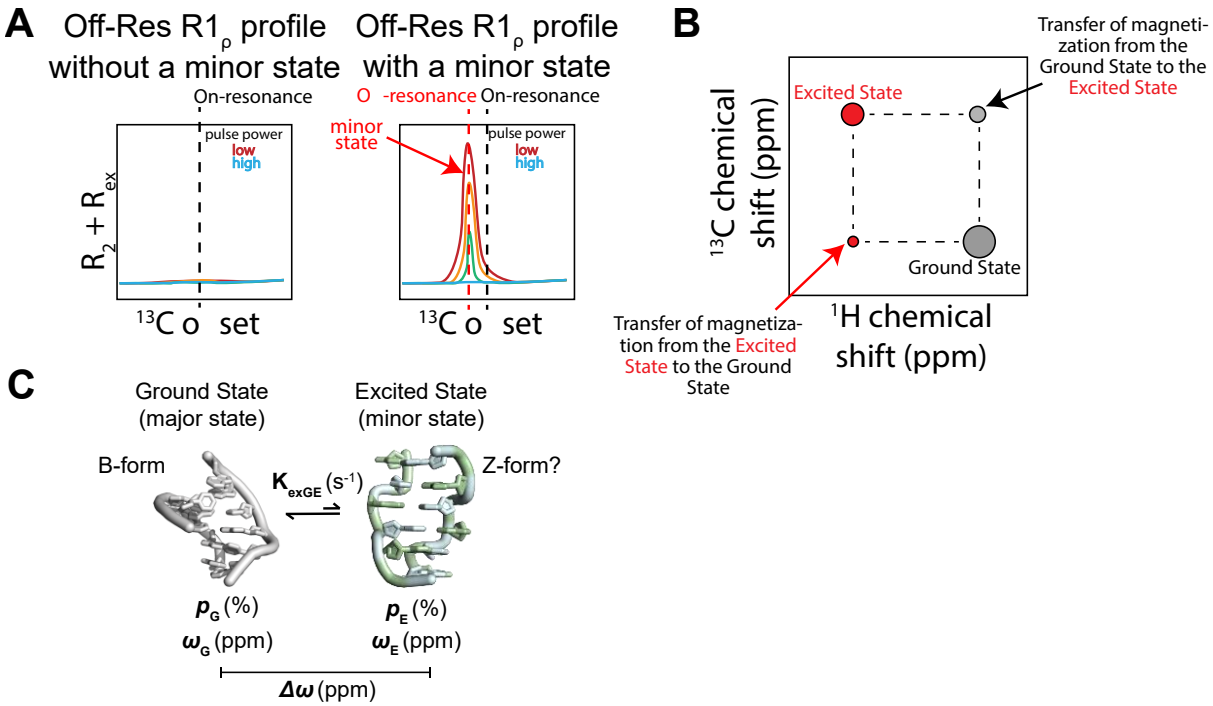

Figure S4. Off-Resonance R1ρ relaxation dispersion experiment for the characterization of excited states in DNA and RNA. (a) Theoretical example Off-Resonance R1ρ relaxation dispersion profile without an excited state (left) and with an excited state on the microsecond-to-millisecond timescale (right). For two-state exchange, the presence of an excited state results in a Gaussian distribution in the $R_2 + R_{ex}$ centered at the chemical shift position of the minor state. As the ^{13}C field-strength of the spin-locking pulse is increased, the relaxation contribution due to chemical exchange is increasingly refocused. This allows for the exchange rate (k_{EXGE}, where G stands for ground state and E stands for excited state), and difference in chemical shift ($\Delta\omega$) between the ground and excited states as well as their populations (p_G and p_E) to be extracted as is depicted in (c). (b) Theoretical example of a ZZ-exchange experiment, where slow exchange between two states can be tracked directly from the buildup of cross-peaks between the diagonal peaks of the two states. Because the exchange is in the slow timescale regime, direct quantification of the diagonal peak intensities and chemical shift values gives the relative populations (p_G and p_E) and chemical shift difference of the two states ($\Delta\omega$), while fitting of the magnetization transfer between the cross-peaks gives the exchange rate (k_{EXGE}). The B-form and Z-form depictions were made using PDBs 1N1K and 2GXB, respectively.

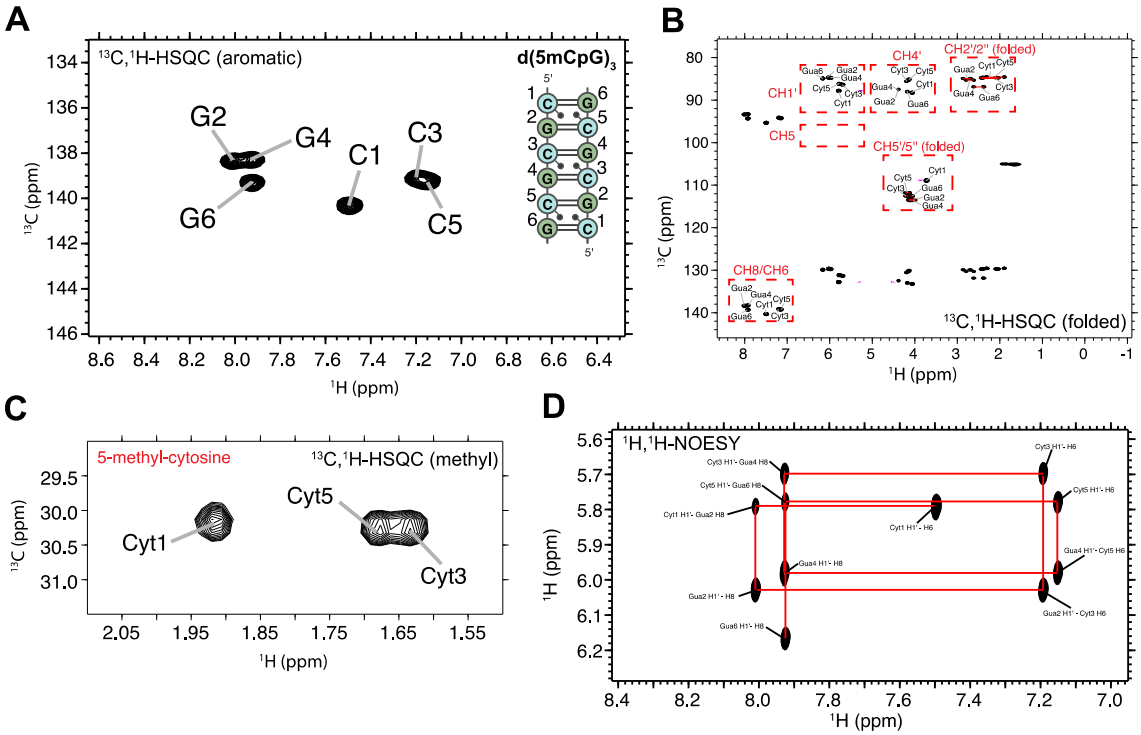

Figure S5. NMR assignment of the d(5mCpG)$_3$ construct. (a) Aromatic ^{13}C-^{1}H HSQC (CH8 of purines and CH6 of pyrimidines) assignments are shown for the d(5mCpG)$_3$ construct (depicted on the right with residue numbering). Note that the two strands of the duplex are chemically equivalent and therefore have identical chemical shifts. (b) Full ^{13}C-^{1}H HSQC spectra assignments are shown. The CH2'/2" and CH5'/5" peak positions are folded in from their normal positions around 40 and 66 ppm, respectively. Their proper chemical shift values are indicated in Table S2. CH3' resonances were not assignable due to water suppression. (c) Methyl ^{13}C-^{1}H HSQC spectra assignments are shown. (d) ^{1}H-^{1}H NOESY experiment with a mixing time of 320 ms showing the aromatic H8/H6 to ribose H1' connectivites. The NOESY "walk" through the B-form helix is indicated with red lines.

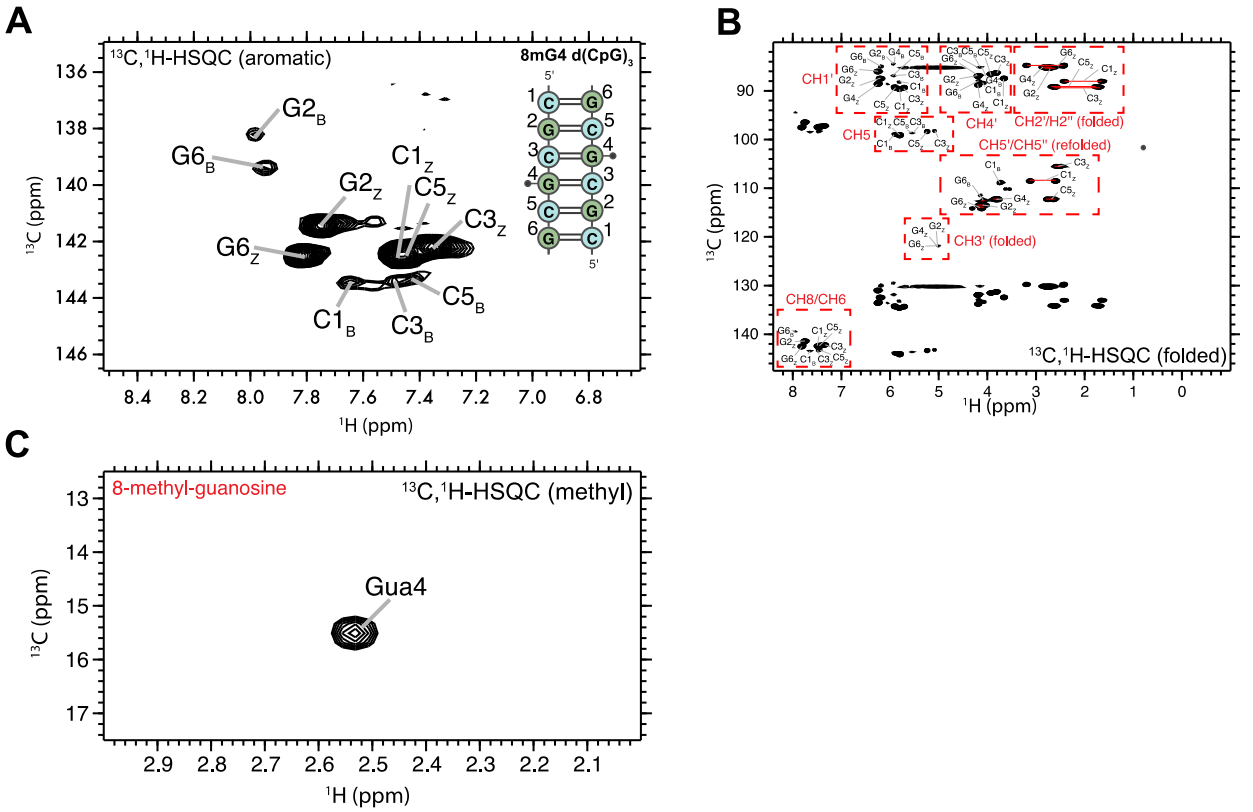

Figure S6. NMR assignment of the 8mG4 d(CpG)$_3$ construct. (a) Aromatic ^{13}C-^{1}H HSQC (CH8 of purines and CH6 of pyrimidines) assignments are shown for the 8mG4 d(CpG)$_3$ construct (depicted on the right with residue numbering). Note that the two strands of the duplex are chemically equivalent and therefore have identical chemical shifts. The 8mG4 d(CpG)$_3$ construct exists in slow exchange between the B- and Z-form. B-form assignments are indicated with the B subscript and Z-form assignments with the Z subscript. (b) Full ^{13}C-^{1}H HSQC spectra assignments are shown. The CH2′/2″, CH3′, and CH5′/5″ peak positions are folded in from their normal positions around 44, 77, and 67 ppm, respectively. Their proper chemical shift values are indicated in Table S3. (c) Methyl ^{13}C-^{1}H HSQC spectra assignment for the 8mG4 is shown. For assignment strategy, see Figure S7.

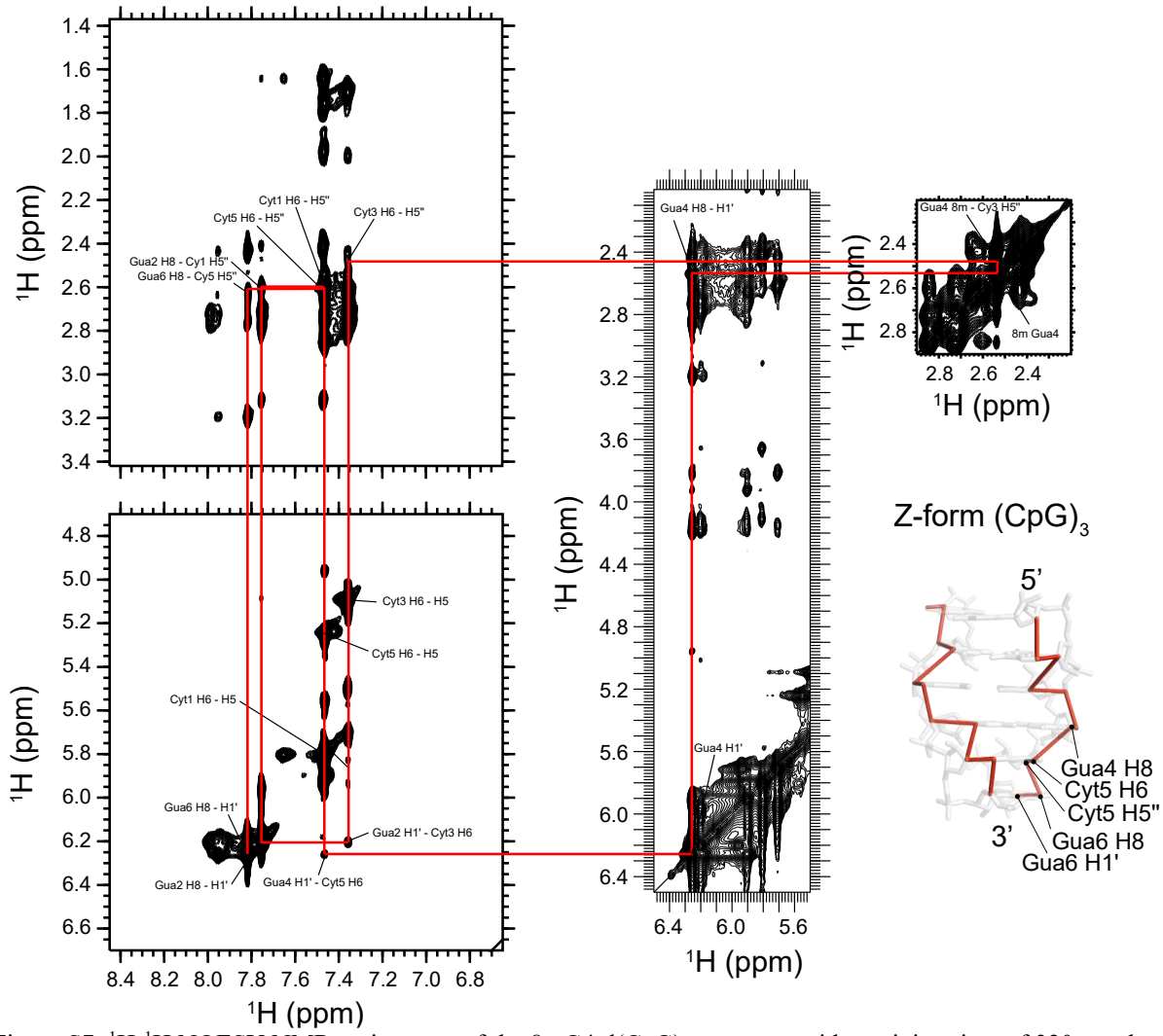

Figure S7. ^{1}H-^{1}H NOESY NMR assignment of the 8mG4 d(CpG)$_3$ construct with a mixing time of 320 ms showing the aromatic H8/H6/8mG4 to ribose H1′ and H5″ connectivites. The NOESY "walk" through the Z-form helix is indicated with red lines, an example of which is shown on the structure of a Z-form helix (PDB: 2GXB) to the right.

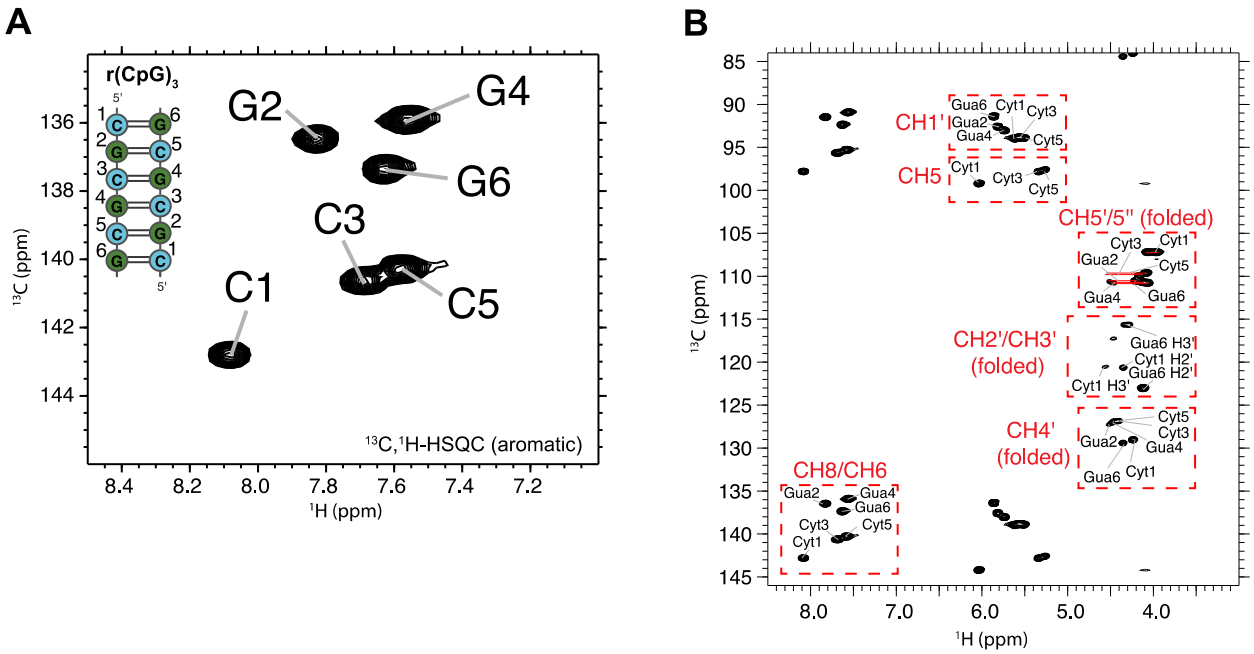

Figure S8. NMR assignment of the r(CpG)$_3$ construct at low salt (A-form). (a) Aromatic ^{13}C-^{1}H HSQC (CH8 of purines and CH6 of pyrimidines) assignments are shown for r(CpG)$_3$ construct (depicted on the left with residue numbering). Note that the two strands of the duplex are chemically equivalent and therefore have identical chemical shifts. (b) Full ^{13}C-^{1}H HSQC spectra assignments are shown. The CH2′, CH3′, CH4′, and CH5′/5″ peak positions are folded in from their normal positions around 75, 73, 83, and 66 ppm, respectively. Their proper chemical shift values are indicated in Table S4. For assignment strategy, see Figure S9.

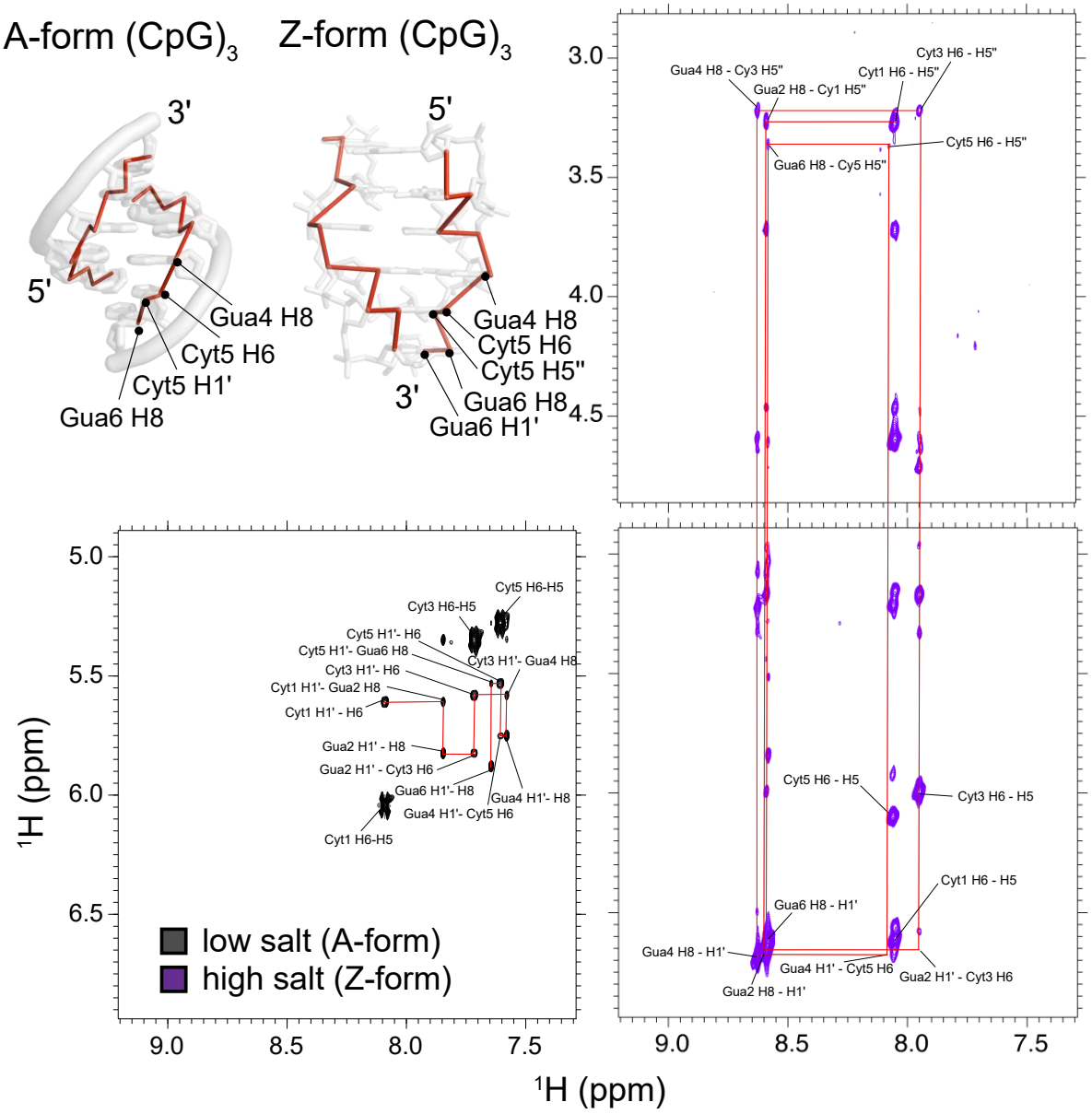

Figure S9. ^{1}H-^{1}H NOESY NMR assignment of the r(CpG)$_3$ construct in low and high-salt with a mixing time of 320 ms showing the aromatic H8/H6 to ribose H1′ (for A-form) and H5″ (Z-form) connectivites. The NOESY "walk" through the A-form (low salt, black peaks) and Z-form (high-salt, purple peaks) helices is indicated with red lines. Example NOESY walks are shown on the structure of an A-form (PDB: 1PBM) and Z-form helix (PDB: 2GXB) in the upper-left.

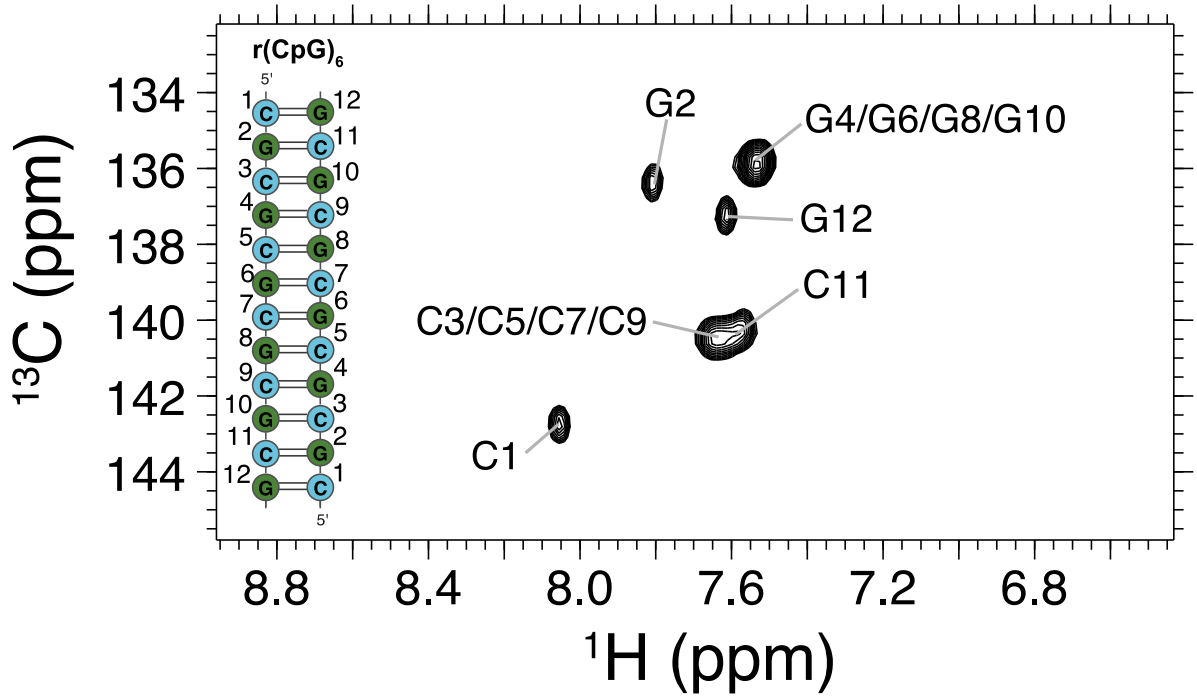

Figure S10. NMR assignment of the r(CpG)$_6$ construct at low salt (A-form). (a) Aromatic ^{13}C-^{1}H HSQC (CH8 of purines and CH6 of pyrimidines) assignments are shown for r(CpG)$_6$ construct (depicted on the left with residue numbering). All residues are overlapped except for residues near the helix ends. Note that the two strands of the duplex are chemically equivalent and therefore have identical chemical shifts. Chemical shift values can be found in Table S5.

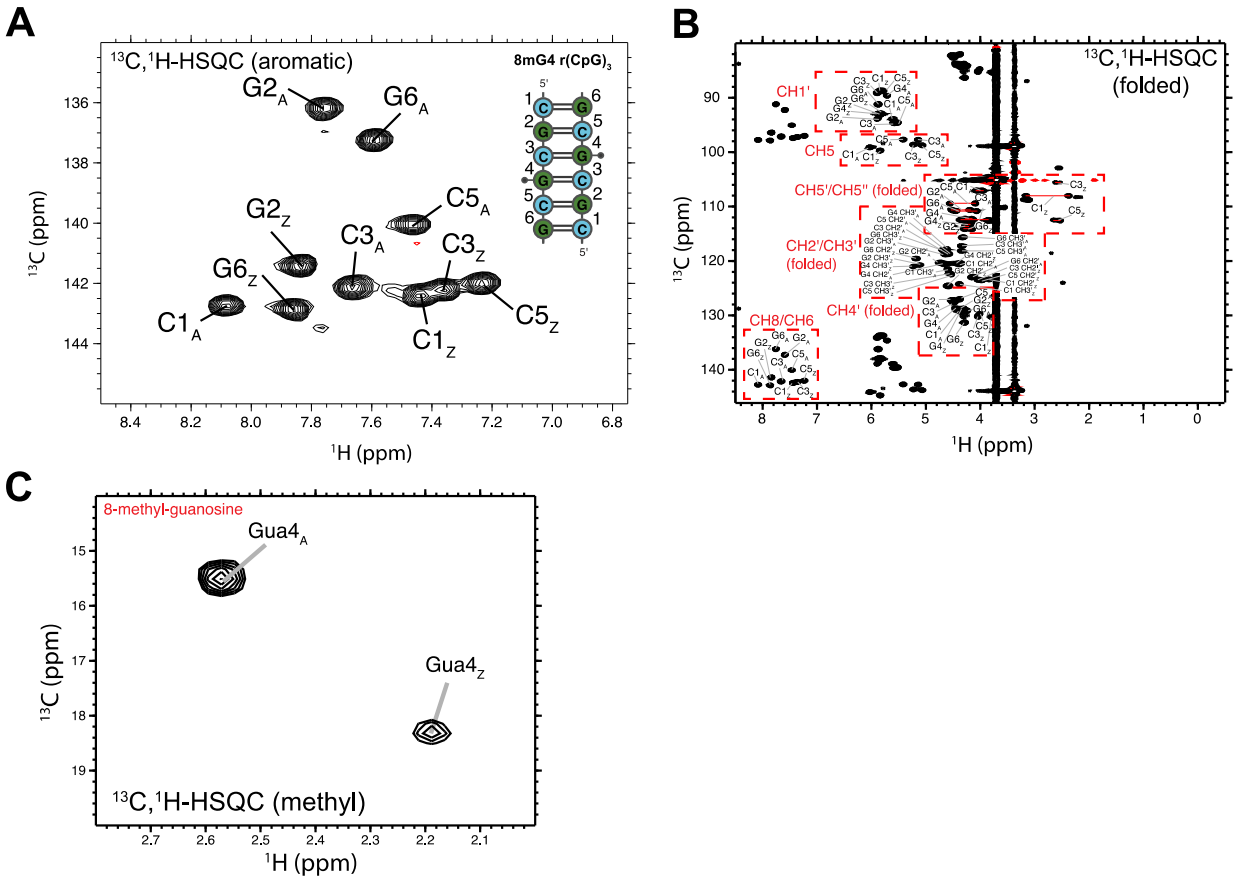

Figure S11. NMR assignment of the 8mG4 r(CpG)$_3$ construct. (a) Aromatic ^{13}C-^{1}H HSQC (CH8 of purines and CH6 of pyrimidines) assignments are shown for 8mG4 r(CpG)$_3$ construct (depicted on the right with residue numbering). Note that the two strands of the duplex are chemically equivalent and therefore have identical chemical shifts. The 8mG4 r(CpG)$_3$ construct exists in slow exchange between the A- and Z-form. A-form assignments are indicated with the A subscript and Z-form assignments with the Z subscript. (b) Full ^{13}C-^{1}H HSQC spectra assignments are shown. The CH2′, CH3′, CH4′, and CH5′/5″ peak positions are folded in from their normal positions around 75, 73, 83, and 66 ppm, respectively. Their proper chemical shift values are indicated in Table S6. (c) Methyl ^{13}C-^{1}H HSQC spectra assignment for the 8mG4 is shown. For assignment strategy, see Figure S12.

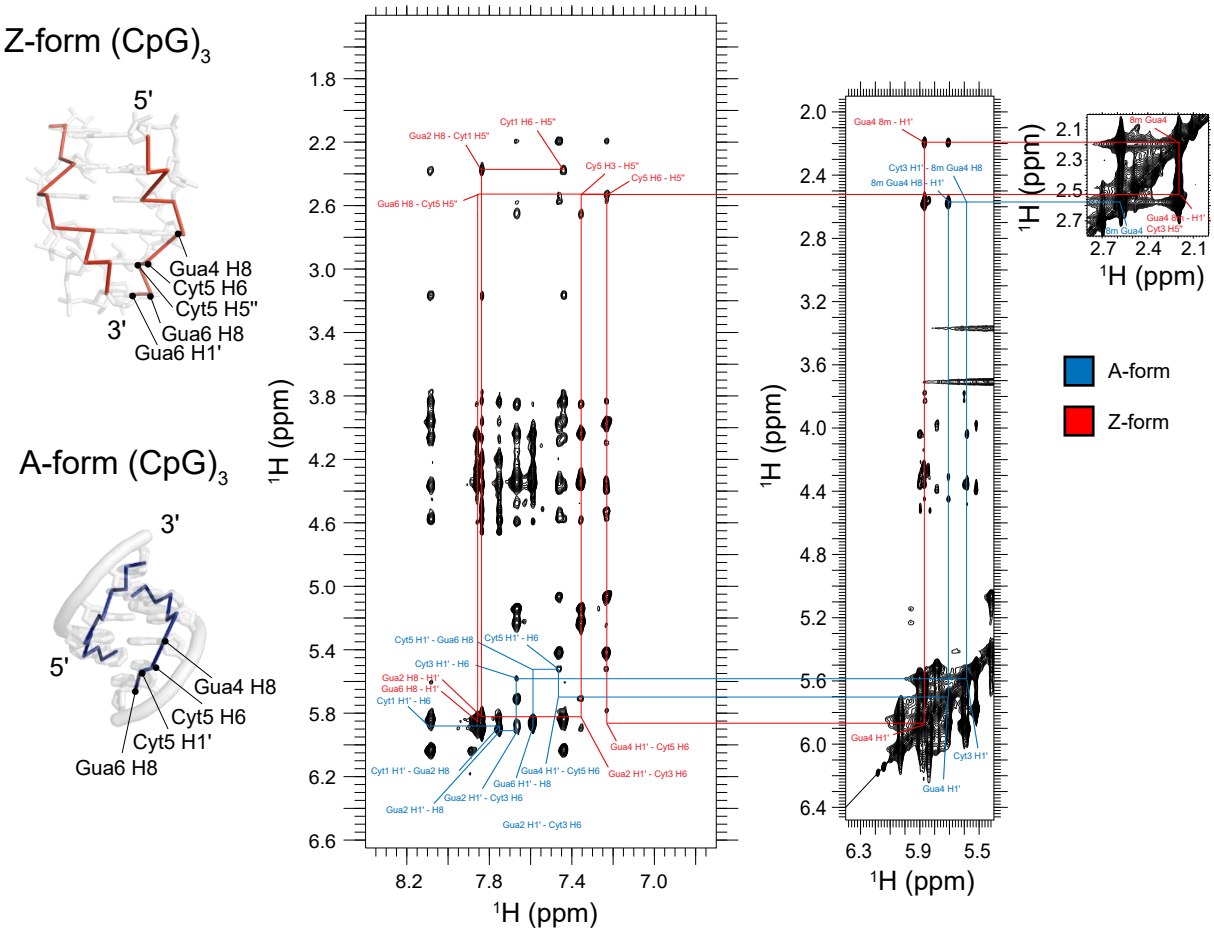

Figure S12. ^{1}H-^{1}H NOESY NMR assignment of the 8mG4 r(CpG)$_3$ construct with a mixing time of 320 ms showing the aromatic H8/H6/8mG4 to ribose H1′ and H5″ connectivites. The NOESY "walk" through the A-form and Z-form helices are indicated with blue and red lines, respectively, an example of which is shown on the structures of an A-form (PDB: 1PBM) and Z-form helix (PDB: 2GXB) on the left.

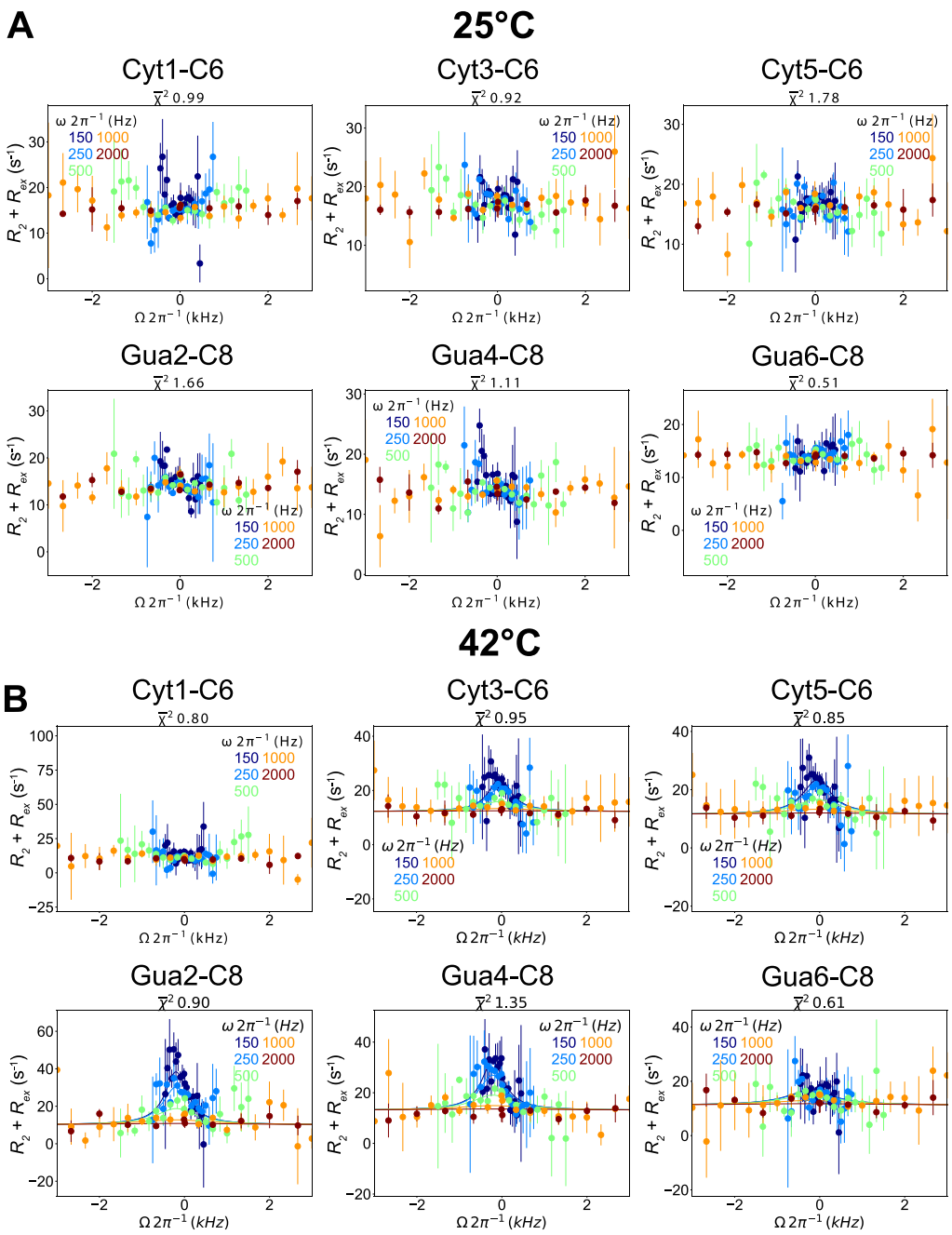

Figure S13. Off-Resonance R1$_\rho$ relaxation dispersion profiles for the aromatic residues of the d(CpG)$_3$ construct at 25°C and 42°C. (a) Off-Resonance R1$_\rho$ relaxation dispersion profiles for C6 and C8 atoms of Cyt1, Gua2, Cyt3, Gua4, Cyt5, and Gua6 carried out at five different spin-lock powers (150, 250, 500, 1000, and 2000 Hz, colored coded according to the legend within each plot). $R_2 + R_{2ex}$ (= $(R_{1\rho} - R_1\cos^2\theta)/\sin^2\theta$, where $\theta = \tan^{-1}$(lock power/offset)) values are given as a function of the resonance offset from the major state ($\Omega_{off}/2\pi$). Error bars represent experimental uncertainty. The fits (solid lines) were carried out as is described in the materials and methods, and extracted parameters from reliable fits are shown in the upper right-hand corner of the plots. (b) the same as (a) except at 42°C.

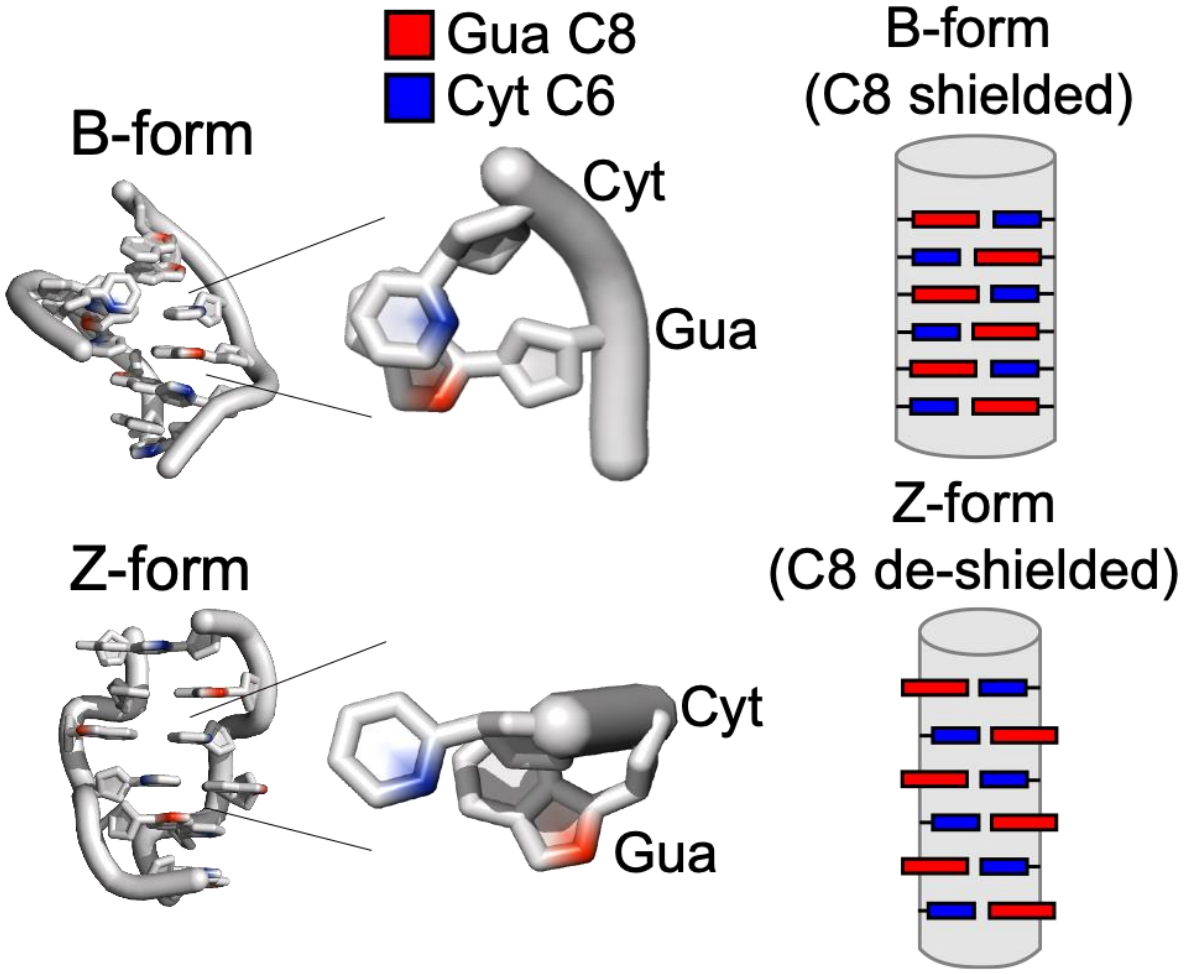

Figure S14. De-shielding of Z-form aromatic purine C8 relative to the A-conformation. The zig-zagged structure of the Z-conformation causes the purine bases in the *syn* conformation to jut out away from the helical axis, thereby resulting in the aromatic C8 atoms to become less shielded compared to the A-conformation, where the bases seamlessly stack on one another. The B-form and Z-form depictions were made using PDB entries 1N1K and 2GXB, respectively.

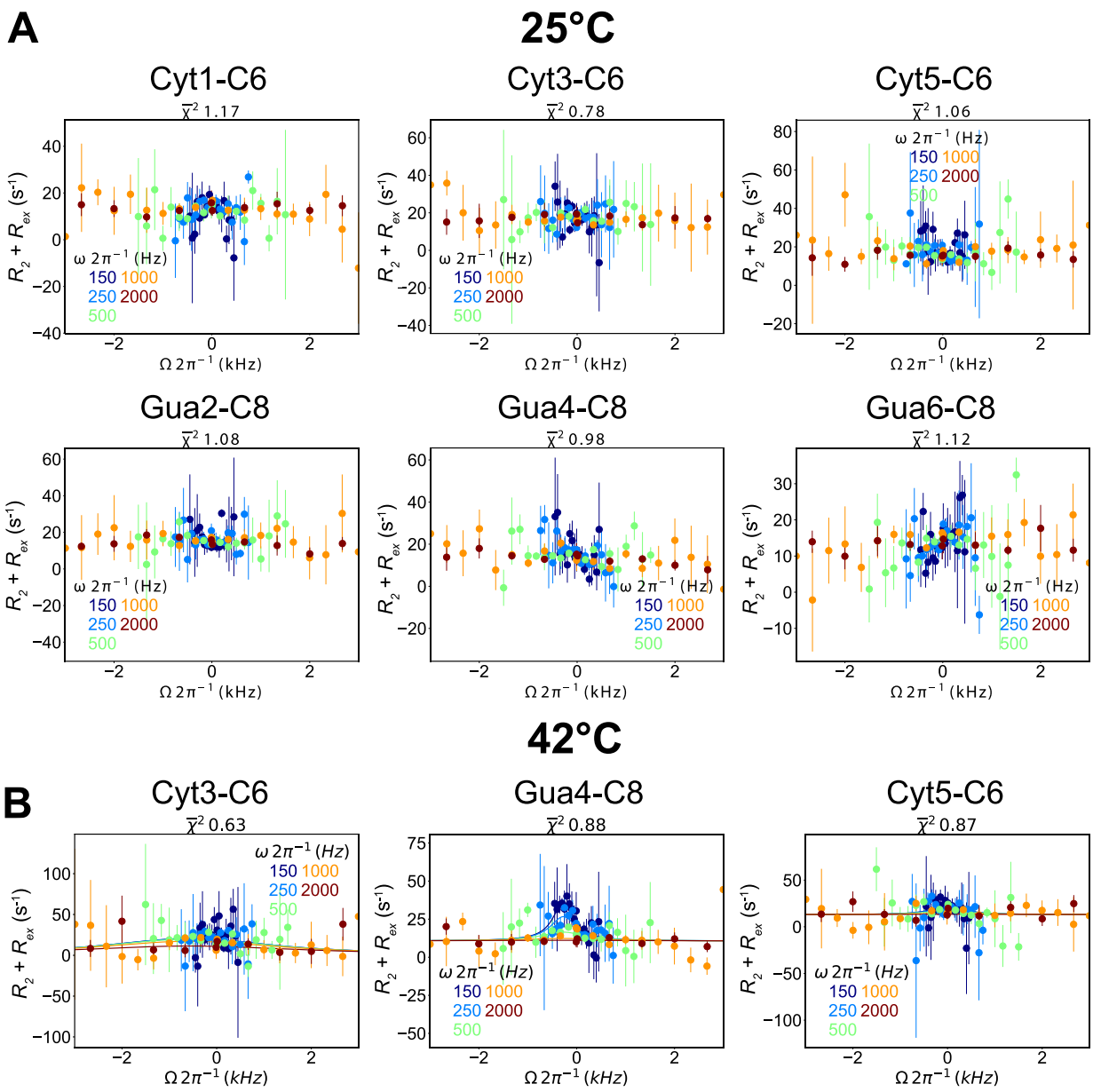

Figure S15. Off-Resonance R1$_\rho$ relaxation dispersion profiles for the aromatic residues of the d(5mCpG)$_3$ construct at 25°C and 42°C. (a) Off-Resonance R1$_\rho$ relaxation dispersion profiles for C6 and C8 atoms of Cyt1, Gua2, Cyt3, Gua4, Cyt5, and Gua6 carried out at five different spin-lock powers (150, 250, 500, 1000, and 2000 Hz, colored coded according to the legend within each plot). $R_2 + R_{2ex}$ (= $(R_{1\rho} - R_1\cos^2\theta)/\sin^2\theta$, where $\theta = \tan^{-1}$(lock power/offset)) values are given as a function of the resonance offset from the major state ($\Omega_{off}/2\pi$). Error bars represent experimental uncertainty. The fits (solid lines) were carried out as is described in the materials and methods, and extracted parameters from reliable fits are shown in the upper right-hand corner of the plots. (b) the same as (a) except at 42°C.

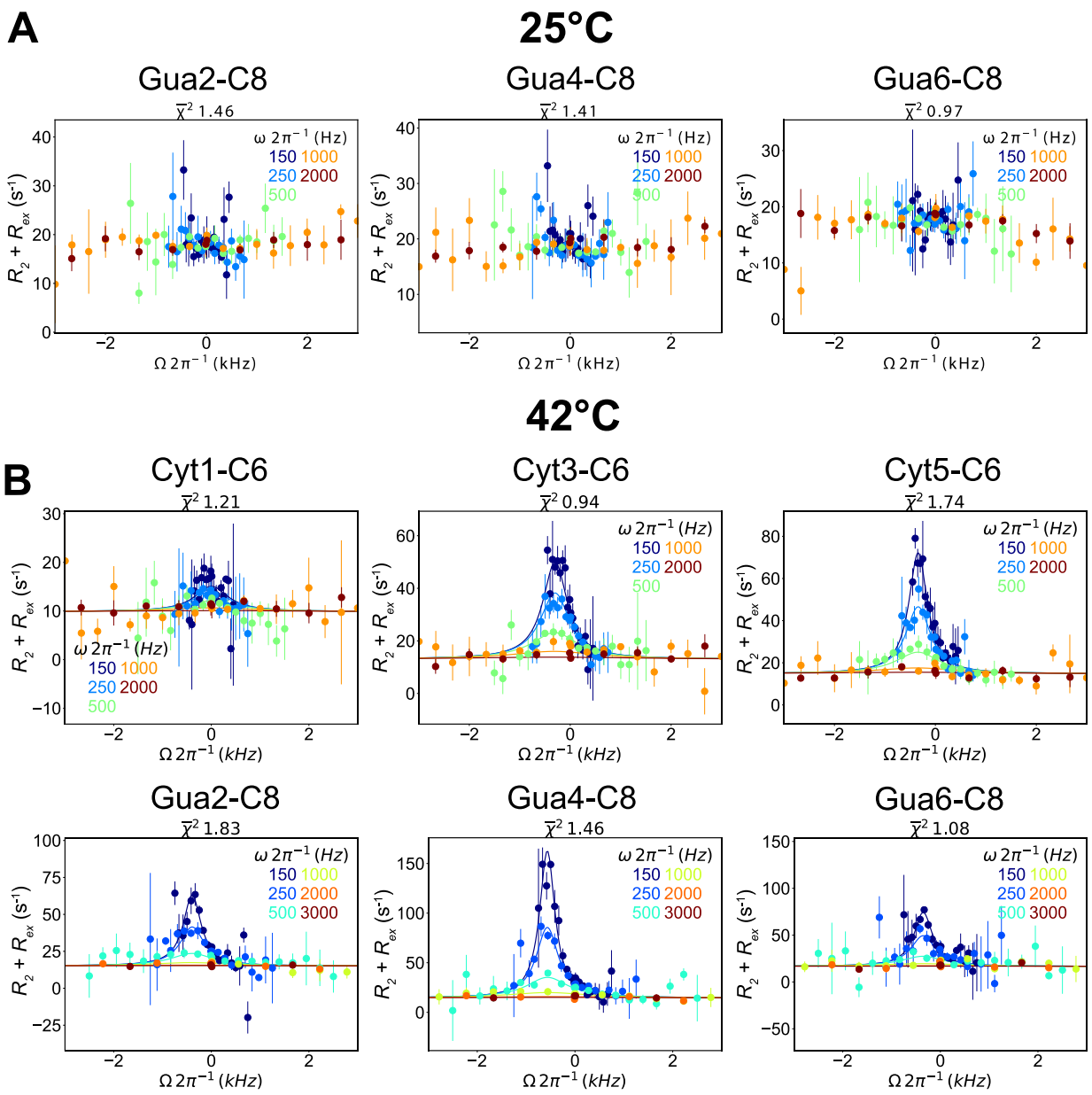

Figure S16. Off-Resonance R1$_\rho$ relaxation dispersion profiles for the aromatic residues of the r(CpG)$_3$ construct at 25°C and 42°C. (a) Off-Resonance R1$_\rho$ relaxation dispersion profiles for C6 and C8 atoms of Cyt1, Gua2, Cyt3, Gua4, Cyt5, and Gua6 carried out at five different spin-lock powers (150, 250, 500, 1000, and 2000 Hz, colored coded according to the legend within each plot). $R_2 + R_{2ex}$ (= $(R_{1\rho} - R_1\cos^2\theta)/\sin^2\theta$, where $\theta = \tan^{-1}$(lock power/offset)) values are given as a function of the resonance offset from the major state ($\Omega_{off}/2\pi$). Error bars represent experimental uncertainty. The fits (solid lines) were carried out as is described in the materials and methods, and extracted parameters from reliable fits are shown in the upper right-hand corner of the plots. (b) the same as (a) except at 42°C.

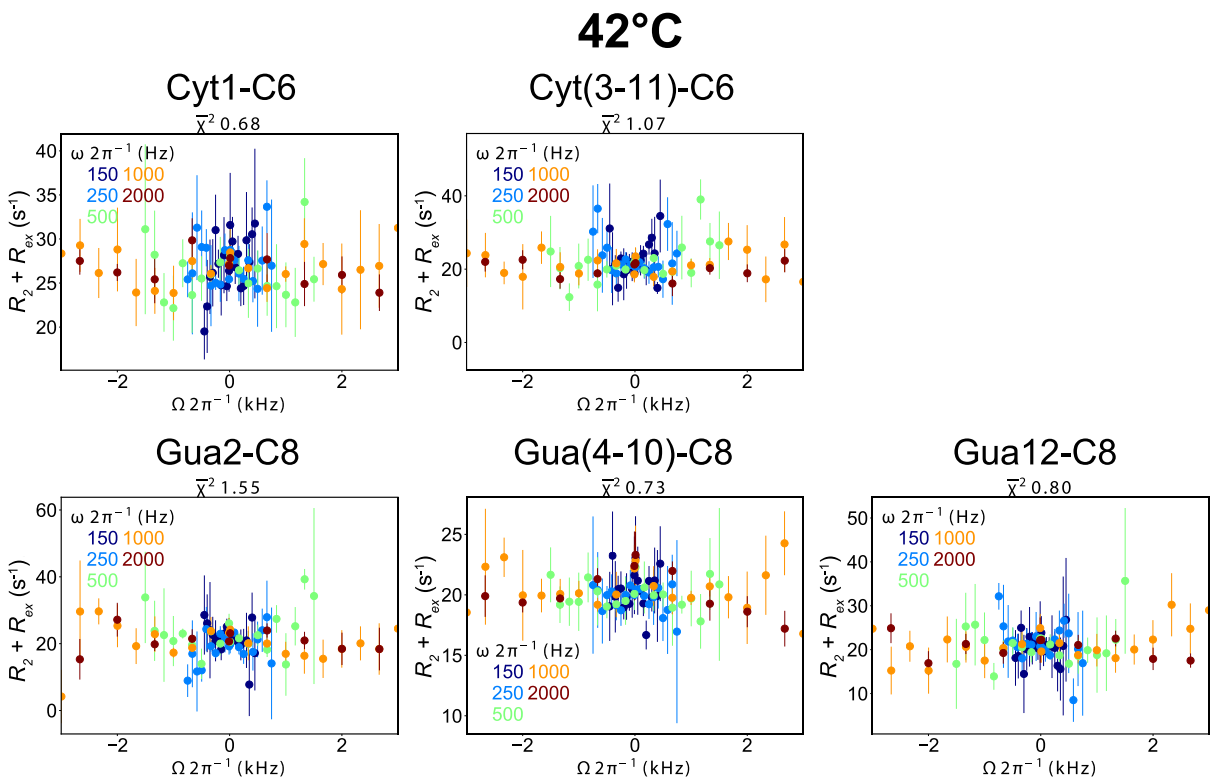

Figure S17. Off-Resonance R1$_\rho$ relaxation dispersion profiles for the aromatic residues of the r(CpG)$_6$ construct at 42°C. Off-resonance R1$_\rho$ Relaxation dispersion profiles for C6 and C8 atoms of Cyt1, Gua2, Cyt3, Gua4, Cyt5, and Gua6 carried out at five different spin-lock powers (150, 250, 500, 1000, and 2000 Hz, colored coded according to the legend within each plot). $R_2 + R_{2ex}$ (= $(R_{1\rho} - R_1\cos^2\theta)/\sin^2\theta$, where $\theta = \tan^{-1}$(lock power/offset)) values are given as a function of the resonance offset from the major state ($\Omega_{off}/2\pi$). Error bars represent experimental uncertainty.

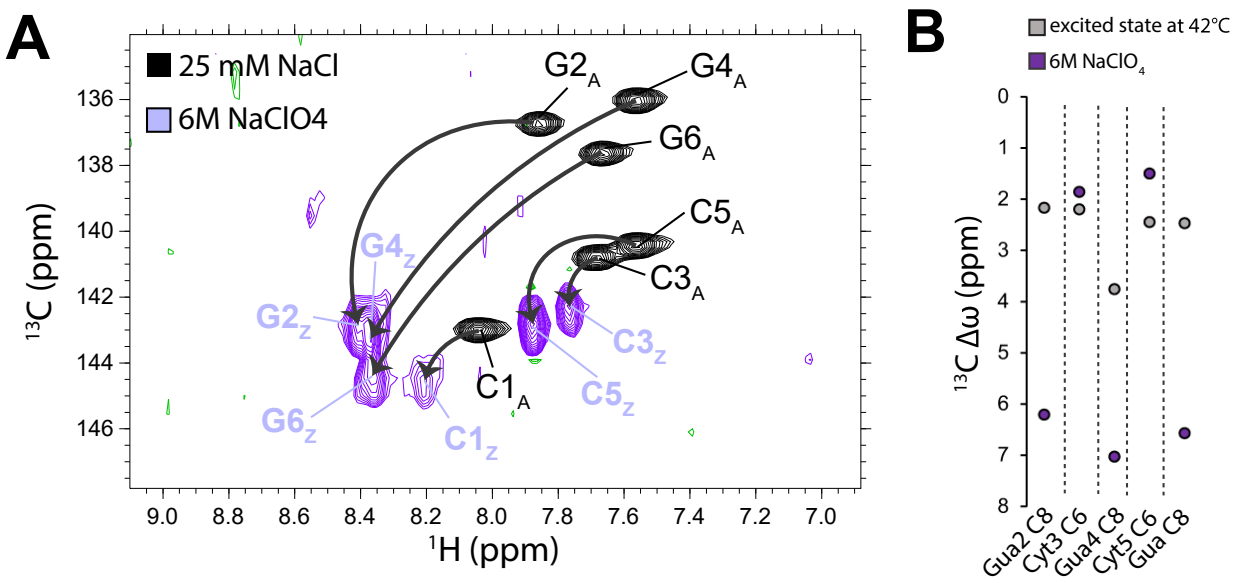

Figure S18. Identification of excited state chemical shift difference extracted from Off-Resonance R1$_\rho$ experiments measured on the r(CpG)$_3$ construct. (a) Aromatic ^{13}C-^{1}H HSQC (CH8 of purines and CH6 of pyrimidines) assignments are shown for r(CpG)$_3$ in 25 mM NaCl (A-form, black peaks) and in 6 M $NaClO_4$ (Z-form, purple peaks. (b) Chemical shift differences (^{13}C $\Delta\omega$) extracted from Off-Resonance R1$_\rho$ experiments measured on the r(CpG)$_3$ construct at 42°C and the chemical shift difference between the A-form and Z-form peaks from the low- and high-salt HSQC spectra from (a).

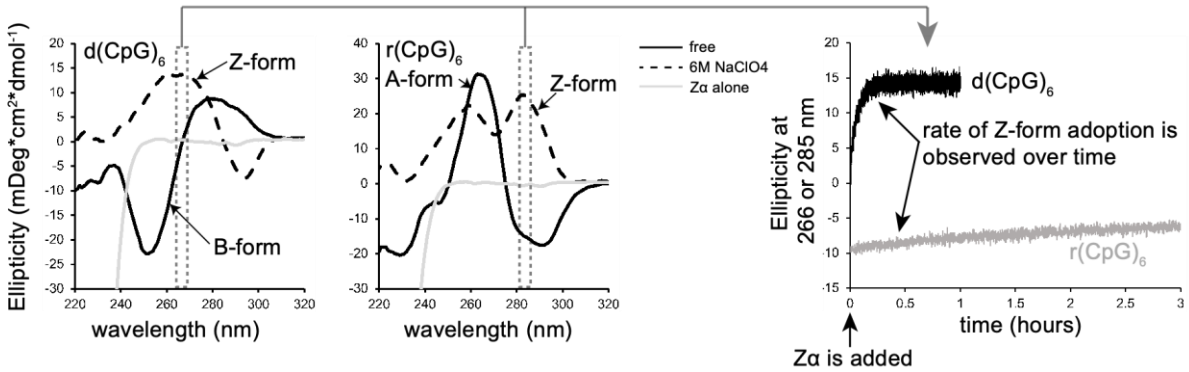

Figure S19. Circular dichroism spectroscopy to track the formation of Z-DNA and Z-RNA. Shown are circular dichroism (CD) spectra from 220 to 320 nm of the $d(CpG)_6$ (left) and $r(CpG)_6$ constructs (at 50 μM) in low salt (B- and A-forms, solid black lines) and 6 M $NaClO_4$ (Z-form, slashed black lines). Zα by itself at a concentration of 400 μM is shown as the solid grey line. The growth in the ellipticity at 266 nm for Z-DNA and 285 nm for Z-RNA can be monitored as a function of time after the addition of Zα to determine the rate of Z-formation adoption (right).

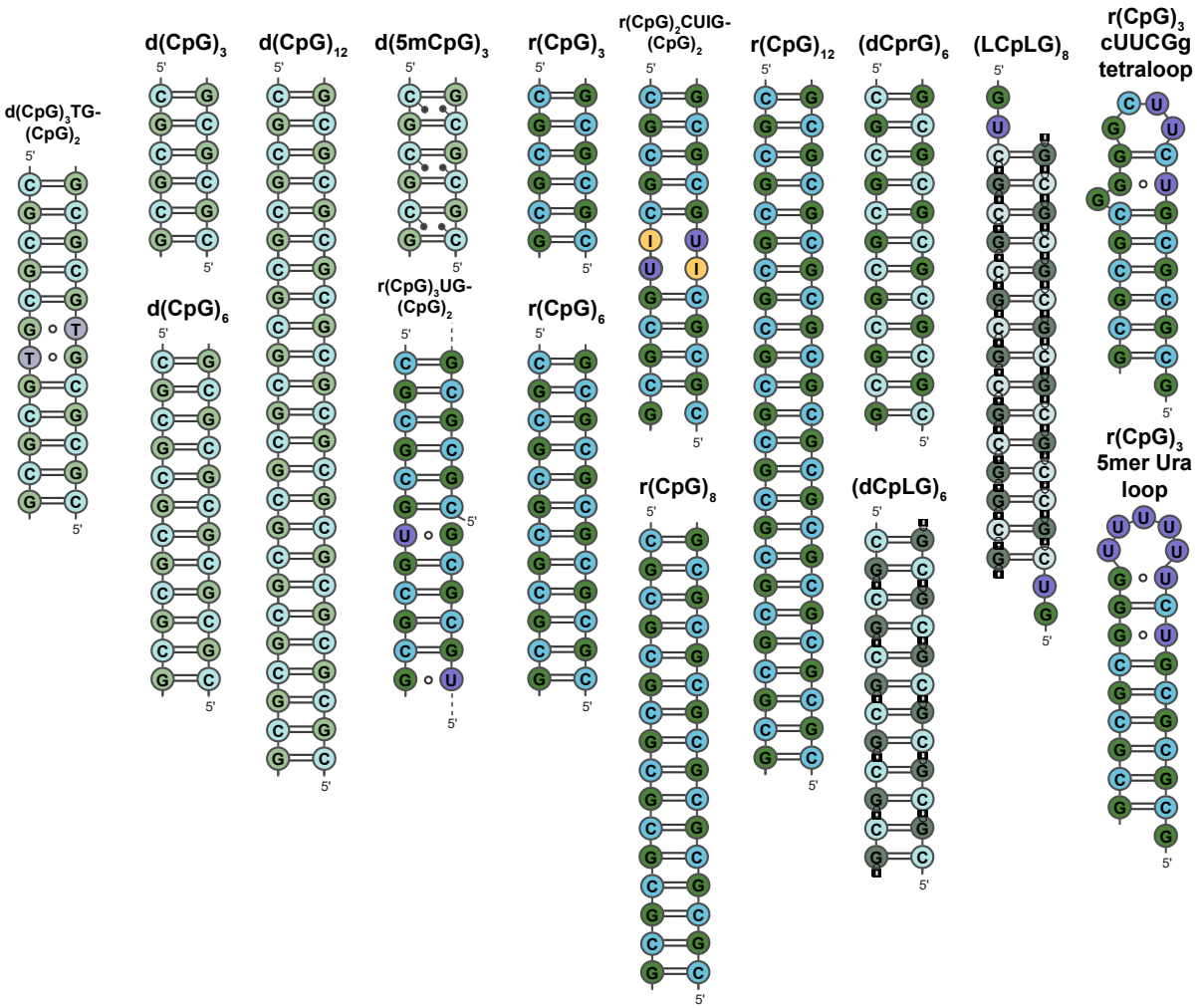

Figure S20. DNA and RNA constructs selected for circular dichroism measurements. 2D representations of the different DNA, RNA, and DNA-RNA hybrid constructs used for CD measurements in this study. DNA bases are more lightly shaded than RNA ones. Methyl groups for the modified constructs are indicated by the small grey circles. The Locked Nucleic Acid (LNA), where all the guanines are locked by a methylene bridge between the 4' carbon and the 2' oxygen thereby locking the sugar pucker conformation into the C3'-endo, is depicted using a lock symbol.

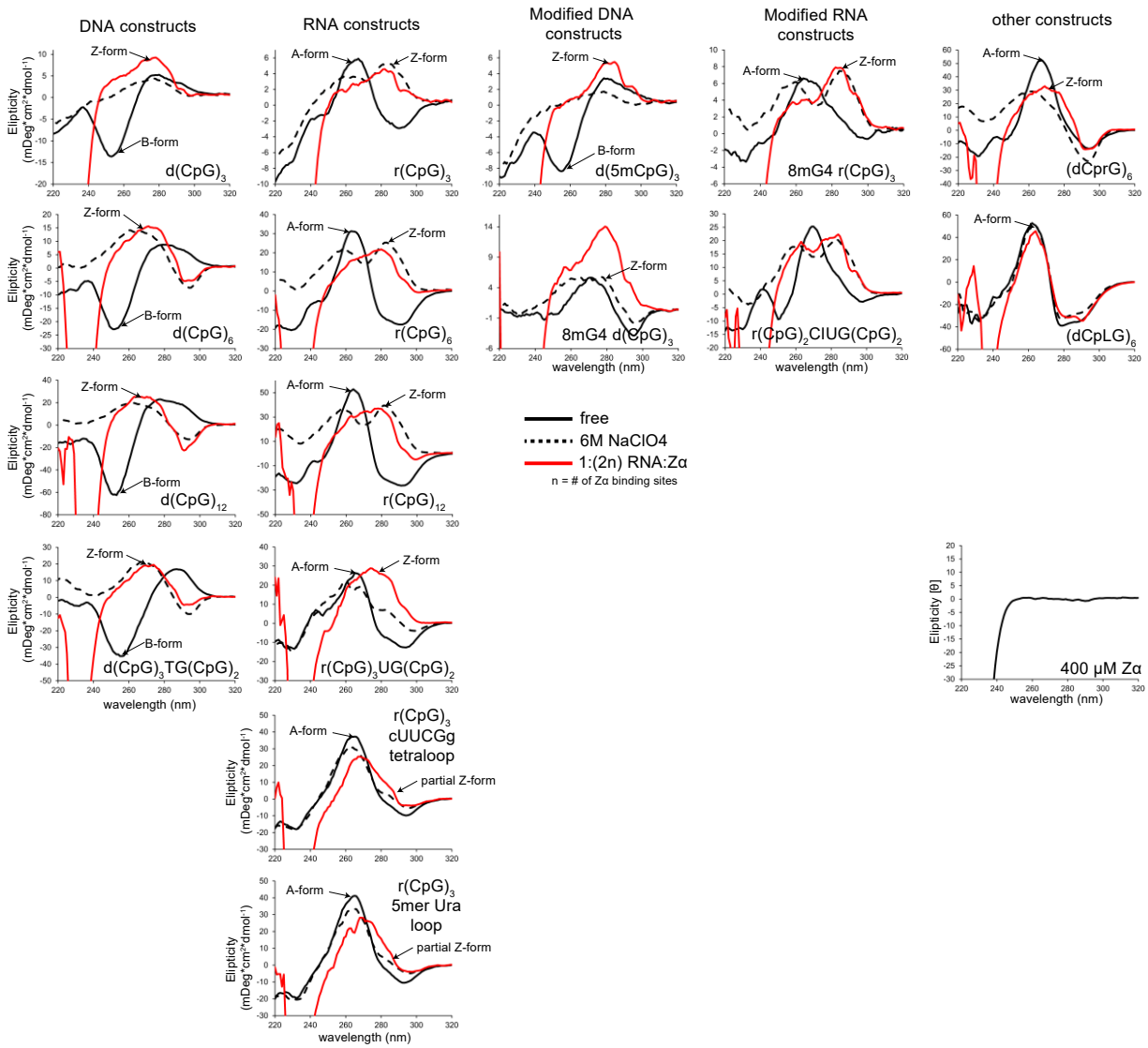

Figure S21. Z-form adoption in DNA, RNA, and DNA-RNA hybrid duplexes measured by circular dichroism. CD spectra from wavelengths of 220 - 320nm of the constructs depicted in Figures 2 and S20 in low salt (free, solid black lines), high-salt (6M NaClO4, dashed black lines), and in complex with Zα (1:[2n] RNA:Zα, where n is the number of Zα binding sites, solid red lines).

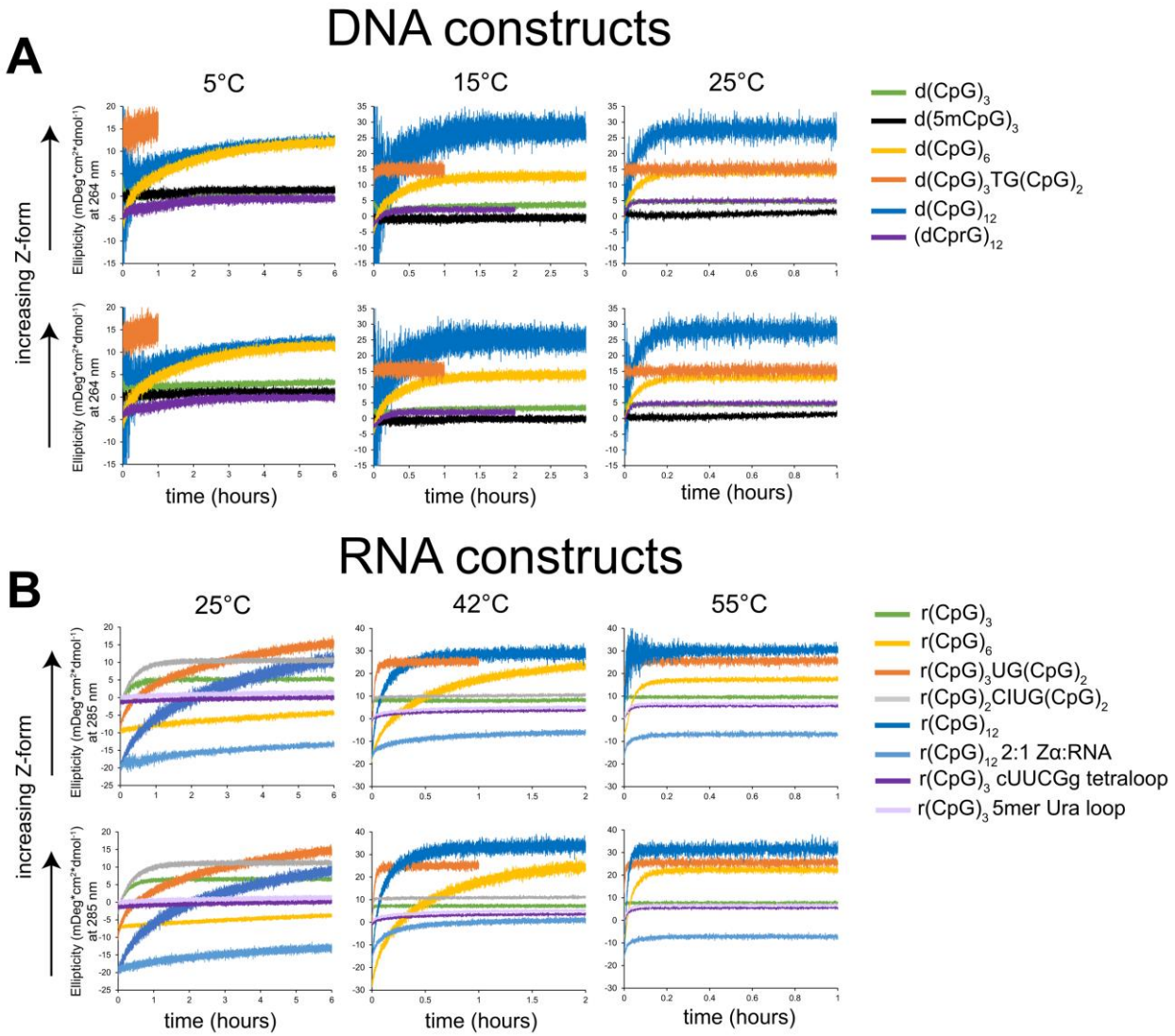

Figure S22. Rates of Z-DNA and Z-RNA adoption in the different constructs. Shown are plots of the ellipticity at 266 nm for Z-DNA (a) and 285 nm for Z-RNA (b) measured by circular dichroism as a function of time after the addition of saturating amounts. (Zα (1:[2n] RNA:Zα where n is the number of Zα binding sites) of Zα, unless specified otherwise. The different constructs are color-coded according to the legend on the right-hand side, and 2D depictions of the constructs are shown in Figure S20. The temperature that the conversion rate was measured at is indicated at the top of the graphs. Each measurement was repeated once (top and bottom graphs). Rate constants were extracted by fitting the data to mono-exponential growth curves, as detailed on the Materials and Methods section.

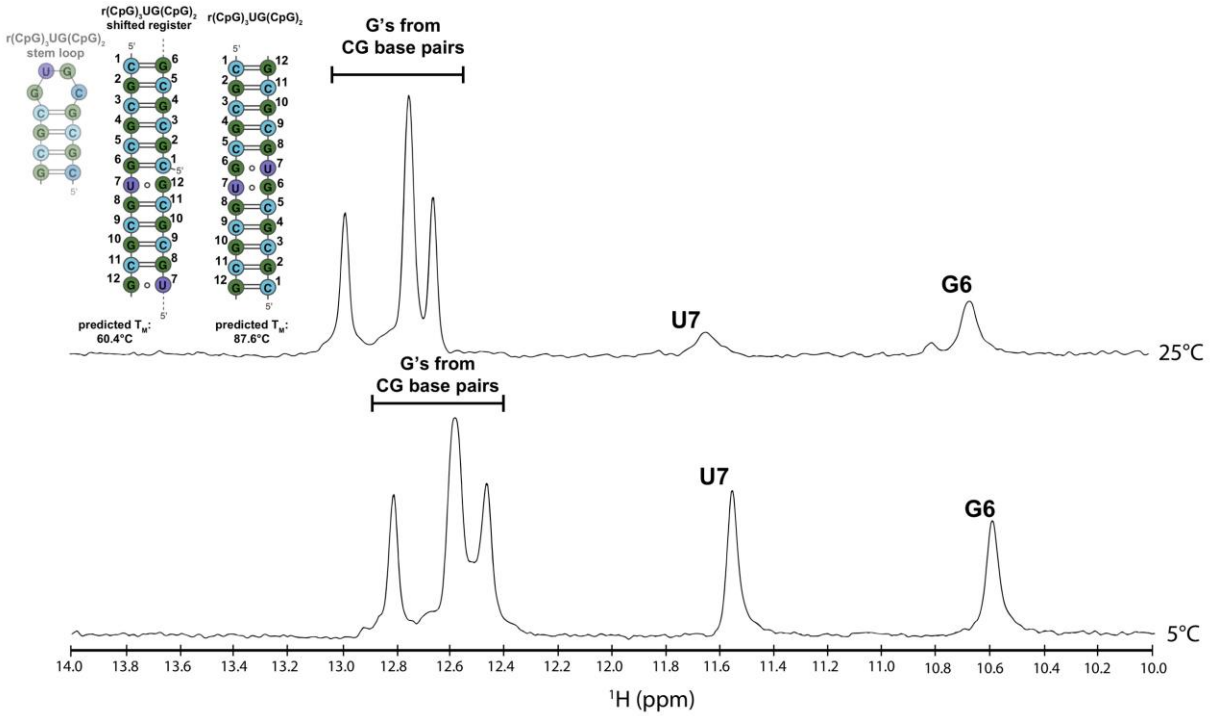

Figure S23. 1D imino NMR spectrum of the r(CpG)$_3$UG(CpG)$_2$ duplex. Shown are the 1D proton imino spectra of the r(CpG)$_3$UG(CpG)$_2$ duplex at 5°C and 25°C. The peaks corresponding to the CG and UG base pairs are indicated. In the upper left are the three possible arrangements of the r(CpG)$_3$UG(CpG)$_2$ duplex. The presence of UG imino peaks means that the stem loop configuration is not possible. The lowered melting temperature of the r(CpG)$_3$UG(CpG)$_2$ relative to the d(CpG)$_3$TG(CpG)$_2$ (Table 1) suggests that the registered shifted configuration is likely the adopted structure in solution.

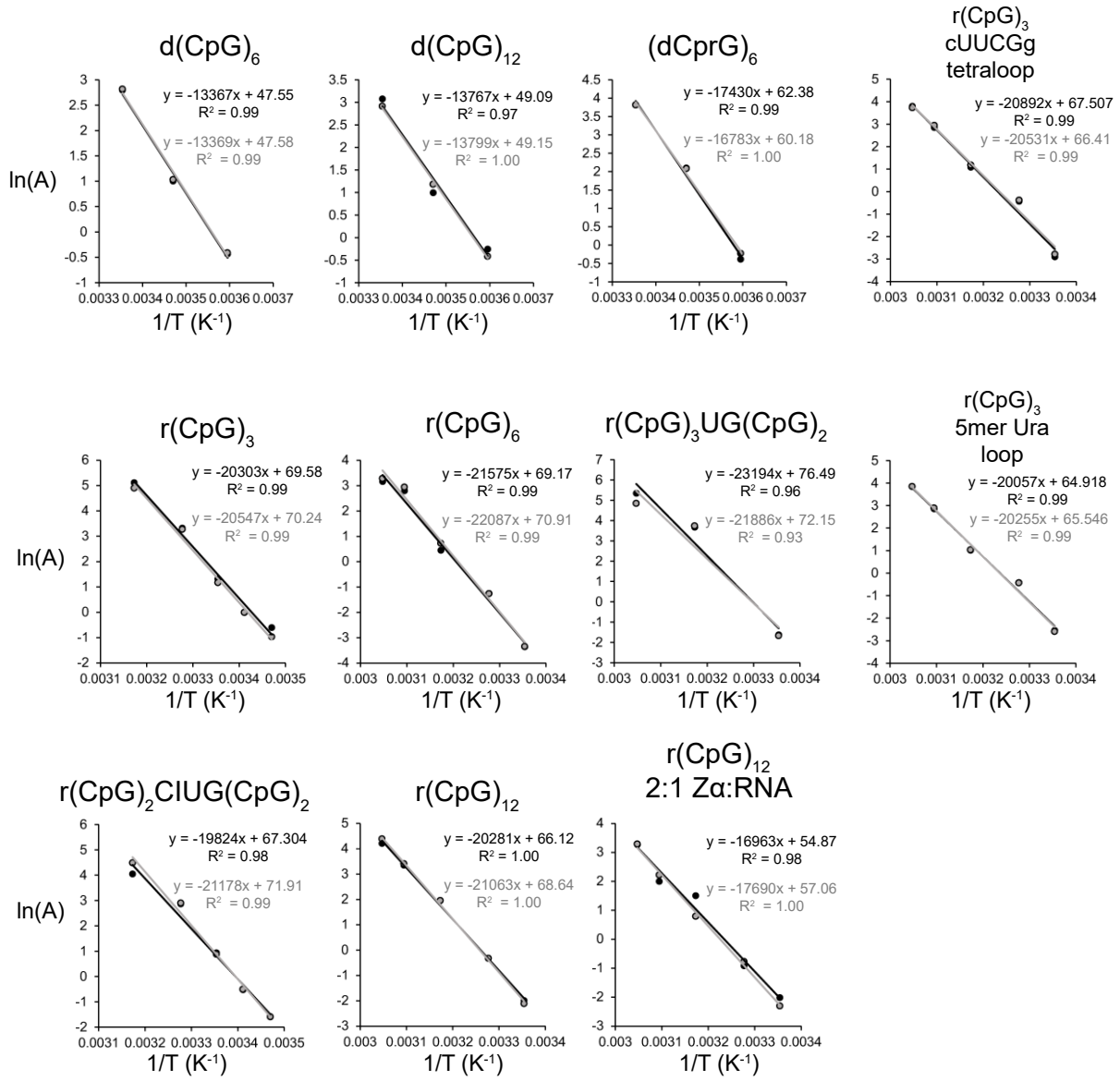

Figure S24. Arrhenius plots from Z-DNA and Z-RNA adoption rates. Arrhenius plots with 1/T (K) on the x-axis and the natural logarithm of the Z-form adoption rate constants (ln(A)) from Figure S22 on the y-axis. The black and grey dots/lines represent two independent measurements. The slope of the linear fits was used to calculate activation energies as detailed in the Materials and Methods section. Extracted activation energies can be found in Table 6.

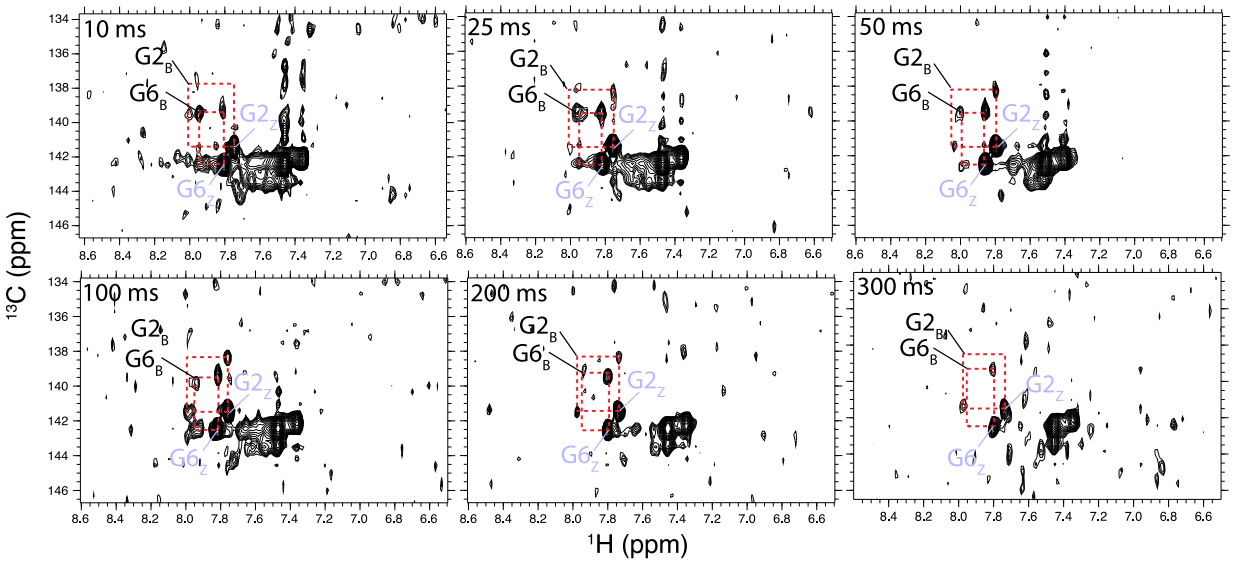

Figure S25. ZZ-exchange NMR spectroscopy measured for the aromatic C8 atoms of the 8mG4 d(CpG)$_3$ construct. ZZ exchange spectra measured at 25°C with mixing times of 10, 25, 50, 100, 200, and 300 ms are shown. The assignments of Guanine 2 and 6 (the only two residues which would be reliably analyzed) are indicated. Fits were carried out as explained in the Materials and Methods Section, and extracted parameters can be found in Table 7.

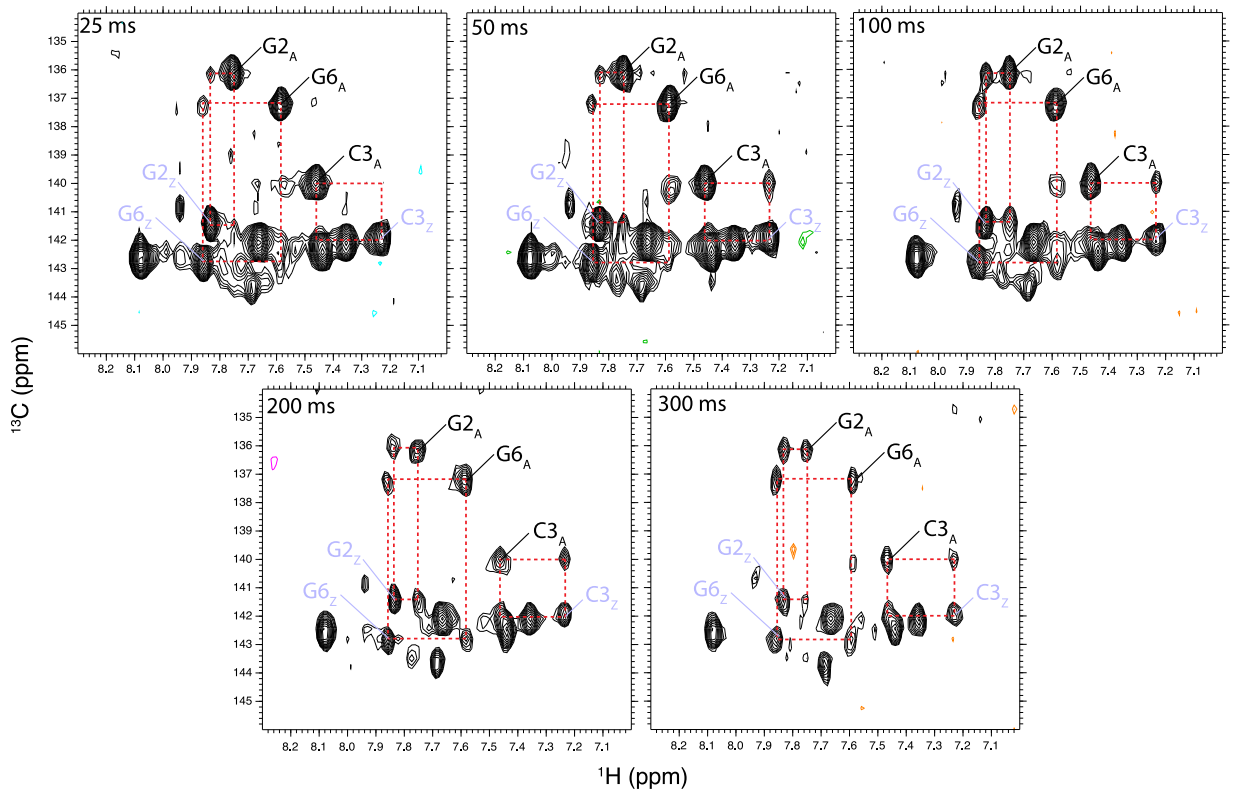

Figure S26. ZZ-exchange NMR spectroscopy measured for the aromatic C6/C8 atoms of the 8mG4 r(CpG)$_3$ construct. ZZ exchange spectra measured at 25°C with mixing times of 25, 50, 100, 200, and 300 ms are shown. The assignments of Guanine 2, Guanine 6, and Cytosine 3 (the only two residues which would be reliably analyzed) are indicated. Fits were carried out as explained in the Materials and Methods Section, and extracted parameters can be found in Table 8.

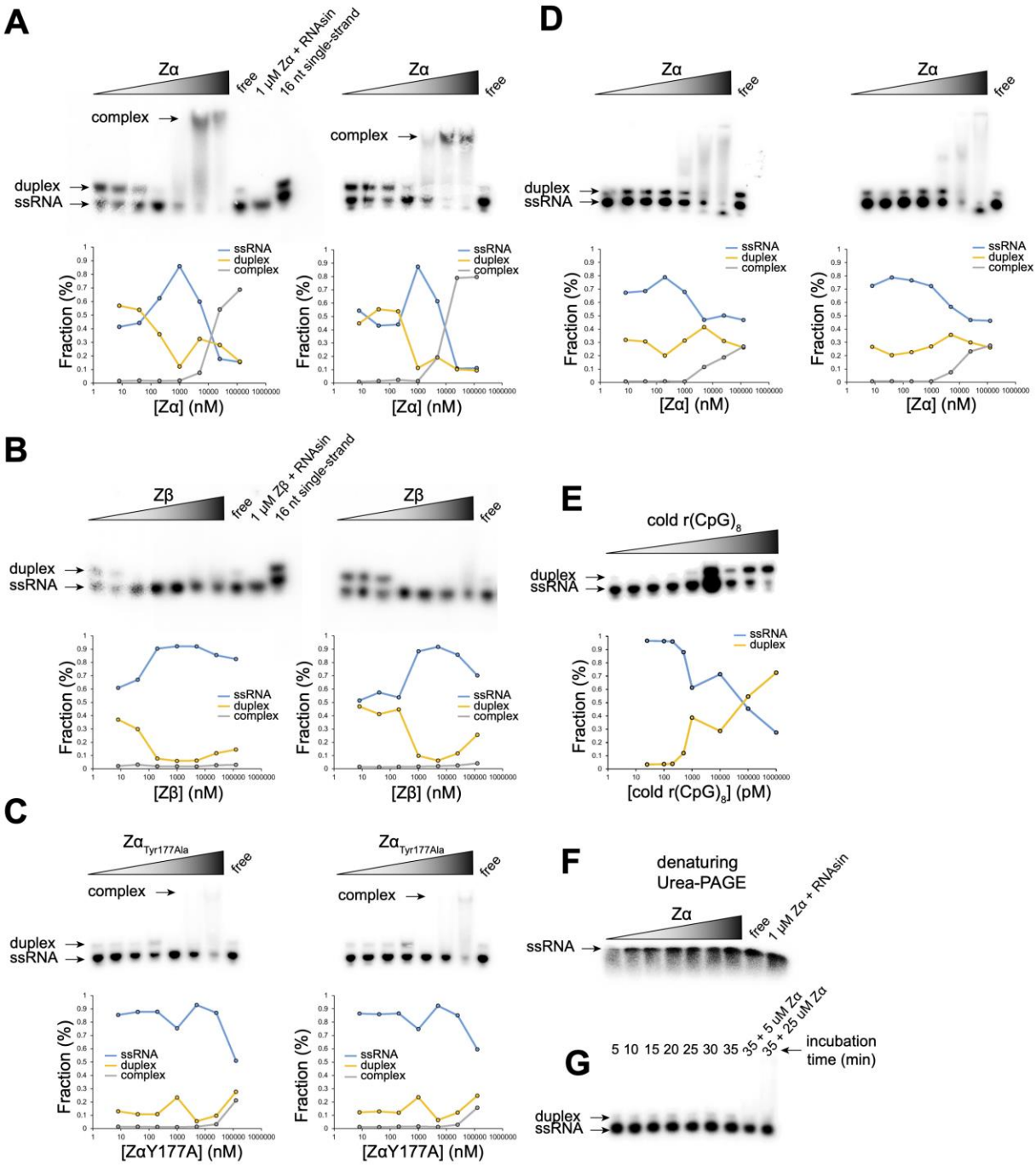

Figure S27. Electrophoretic mobility shift assays of Zα, Zβ, and ZαY177A binding to a γ-^{32}P-labeled r(CpG)$_8$ construct. (a) The binding of Zα to the r(CpG)$_8$ duplex by EMSA is shown. The lanes (from left to right) are as follows: 8 nM Zα, 40 nM Zα, 200 nM Zα, 1 μM Zα, 5 μM Zα, 25 μM Zα, 125 μM Zα, 0 μM Zα, and 1 μM Zα + 1 μL RNAsin. The last lane is not the r(CpG)$_8$ but a 16 nt GGUUUAUGGCGCGCG RNA without its complement strand. The location of the ssRNA, dsRNA, and complex is indicated. Each EMSA was repeated once (duplicates are shown left and right). The intensity of the bands was quantified and the fraction of the ssRNA, dsRNA, and complex is shown below the gels on a log scale. (b) same as in (a) except using Zβ. (c) same as in (a) except using a mutant version of Zα where the critical tyrosine 177 is mutated to alanine. (d) EMSA of the γ-^{32}P-labeled labeled r(CpG)$_8$ duplex with increasing concentrations of unlabeled r(CpG)$_8$. The concentrations of unlabeled r(CpG)$_8$ increase from left to right: 0, 25 pM, 100 pM, 200 pM, 500 pM, 1 nM, 10 nM, 100 nM, and 1 μM). (e) same as in (a) but under denaturing conditions (7 M Urea). (f) Same as in a-c, but with the (CpG)$_8$ LNA construct which cannot adopt the Z-conformation.

(g) EMSA time-course for the γ-^{32}P-labeled r(CpG)$_8$ RNA with 1 μM of Zα over a period of 5 to 35 minutes. The last two lanes are r(CpG)$_8$ RNA which was incubated with 1 μM of Zα for 30 minutes) and then had either 5 or 25 μM Zα added before loading the gels. There was a 5 minute deadtime to load the gels.